Atmospheric
Chemistry
and Physics
Discussions

Open Access

EGU

1 Volcanic ash modeling with the on-line NMMB/BSC-ASH-

2 v1.0 model: model description, case simulation and

3 evaluation

4 **Alejandro Marti [(1)(*)], Arnau Folch [(1)], Oriol Jorba [(1)] and Zavisa Janjic [(2)]**

5 [1]{Barcelona Supercomputing Center (BSC-CNS), Barcelona, Spain}

6 [2]{National Center for Environmental Prediction, College Park, Maryland, USA}

7 (*) Correspondence to: Alejandro Marti (Alejandro.Marti@bsc.es)

8

9 **Abstract**

10 Traditionally, tephra transport and dispersal models have evolved decoupled (off-line) from numerical weather

11 prediction models. There is a concern that inconsistencies and shortcomings associated to this coupling strategy

12 might lead to errors in the ash cloud forecast. Despite this concern, and the significant progress to improve the

13 accuracy of tephra dispersal models in the aftermath of the 2010 Eyjafjallajökull and 2011 Cordón Caulle

14 eruptions, to date, no operational on-line dispersal model is available to forecast volcanic ash. Here, we describe

15 and evaluate NMMB/BSC-ASH, a new on-line multiscale meteorological and transport model that attempts to

16 pioneer the forecast of volcanic aerosols at operational level. The model predicts volcanic ash cloud trajectories,

17 concentration of ash at relevant flight levels, and the expected deposit thickness for both regional and global

18 configurations. Its on-line coupling approach improves the current state-of-the-art of tephra dispersal models,

19 especially in situations where meteorological conditions are changing rapidly in time, two-way feedbacks are

20 significant, or distal ash cloud dispersal simulations are required. This work presents the model application for

21 the first phases of the 2011 Cordón Caulle and 2001 Mt. Etna eruptions. The computational efficiency of

22 NMMB/BSC-ASH and its application results compare favorably with other long-range tephra dispersal models,

23 supporting its operational implementation.

24

25 **Keywords:** volcanic ash, on-line coupling, transport-meteorological modeling, operational forecast, NWPM,

26 TTDM, Cordón Caulle, Mt. Etna.

27

28

29

30

1

Atmospheric
Chemistry
and Physics
Discussions

1 Introduction

Explosive volcanic eruptions can eject large quantities of particulate matter (tephra) that, along with other aerosol droplets and trace gases, are carried upwards into the atmosphere by the buoyant eruption column and then dispersed by winds aloft (e.g. Sparks et al., 1997). Tephra particles smaller than 2 mm in diameter, technically defined as volcanic ash (Schmid, 1981), can spread over large distances away from the source forming ash clouds that jeopardize air-traffic (Casadevall, 1993), airports (Guffanti et al., 2009) and, for very large eruptions, alter both atmospheric composition and chemistry (Myhre et al., 2013; Self, 2006). Tephra Transport and Dispersal Models (TTDMs, e.g. Folch, 2012) are used to simulate the atmospheric transport, dispersion and ground deposition of tephra, and to generate operational short-term forecasts to support civil aviation and emergency management. The recent eruptions of Eyjafjallajökull (Iceland) in 2010 and Cordón Caulle (Chile) in 2011 have reinforced the importance of tephra dispersal in the context of global aviation safety. In addition to short-term forecast, other model applications include the reconstruction of past events, studying the impact of volcano eruptions on climate, probabilistic tephra hazard assessments or simulation of recent eruptions for model evaluation purposes. For any of those cases, TTDMs require a driving Numerical Weather Prediction Model (NWPM) or a meteorological reanalysis dataset for the description of the atmospheric conditions, and an emission or source model for the characterization of the eruption column (Fig. 1).

Traditionally, TTDMs have evolved decoupled (off-line) from NWPMs. In the off-line strategy, the meteorological driver runs *a priori* and independently of the TTDM to produce the required meteorological fields at regular time slabs (e.g. hourly). Meteorological data is then furnished to the TTDM, which commonly assumes constant values for the meteorological fields during each time slab or, at most, performs a linear interpolation in time. Although the off-line approach is operationally advantageous, there is a concern that it can lead to a number of accuracy issues (e.g. inaccurate handling of atmospheric processes) and limitations (e.g. neglect of feedback effects) that can be corrected by on-line approaches (Grell et al., 2004). These inconsistencies are especially important when meteorological conditions change rapidly in time or for long-range transport. However, uncertainties arising from off-line systems have received little attention, even if the experience from other communities (e.g. air quality) highlights the importance of coupling on-line dispersal and meteorological models (e.g. Grell and Baklanov, 2011). To date, only the Weather Research and Forecasting model with couple Chemistry (WRF-Chem; Grell et al., 2005) includes a coupled functionality that allows simulating emission, transport, dispersion, transformation and sedimentation of pollutants released during volcanic activities (Stuefer et al., 2012).

In this paper we describe and evaluate NMMB/BSC-ASH, a new on-line meteorological and atmospheric transport model to simulate the emission, transport and deposition of ash (tephra) particles released from volcanic eruptions. The model predicts ash cloud trajectories, concentration of ash at relevant flight levels, and the expected deposit thickness for both regional and global domains. The novel on-line coupling in NMMB/BSC-ASH allows solving both the meteorological and aerosol transport concurrently and interactively at every time-step. This coupling strategy aims at improving the current state-of-the-art of tephra dispersal models, especially in situations where meteorological conditions are changing rapidly in time, two-way feedbacks are significant, or distal ash cloud dispersal simulations are required. The model builds on the NMMB/BSC Chemical Transport Model (NMMB/BSC-CTM; Jorba et al., 2012; Pérez et al., 2011) to represent the transport

2

Atmospheric
Chemistry
and Physics
Discussions

1   of volcanic particles. Its meteorological core, the Non-hydrostatic Multiscale Model on a B grid (NMMB; Janjic

2   and Black, 2007; Janjic and Gall, 2012; Janjic, 2005; Janjic et al., 2011), allows for nested global-regional

3   atmospheric simulations by using consistent physics and dynamics formulations. The final objective in

4   developing NMMB/BSC-ASH is two-fold. On one hand, at a research level, we aim at studying the differences

5   between the on-line/off-line modeling strategies. Moreover, a second version of the model is projected to

6   quantify the feedback effects of dense volcanic ash clouds from large explosive eruptions on the radiative budget

7   and local meteorology. On the other hand, at an operational level, the low computational cost of the NMMB

8   dynamic core suggests that NMMB/BSC-ASH could be applied for more accurate on-line operational

9   forecasting of volcanic ash clouds. Consequently, the focus on developing an on-line volcanic ash model is

10   timely.

11   This manuscript is arranged as follows: Section 2 summarizes the modeling background and the standard

12   physical schemes employed in NMMB/BSC-ASH; Section 3 provides a comprehensive description of the ash

13   related modules, including details about the emission, transport, and deposition of volcanic particles; Section 4

14   validates the regional and global configurations of the model with simulations for the 2001 Mt. Etna and 2011

15   Cordón Caulle long-lasting eruptions; Section 5 discusses the implementation of the model for its operational

16   use and; finally, Section 6 provides a summary conclusion of this work.

17

18   **2   Modeling background**

19   NMMB/BSC-ASH is a novel on-line multi-scale meteorological and atmospheric transport model developed at

20   the Barcelona Supercomputing Center (BSC). The model attempts to pioneer the forecast of volcanic aerosols by

21   embedding a series of new modules on the BSC's operational system for short/mid-term chemical weather

22   forecasts (NMMB/BSC-CTM) developed at the BSC in collaboration with the U.S National Centers for

23   Environmental Prediction (NCEP) and the NASA Goddard Institute for Space Studies. The development of the

24   volcanic ash module follows the implementation of the mineral dust (Pérez et al., 2011) and sea-salt (Spada et

25   al., 2013) modules in NMMB/BSC-CTM, and allows for a range of different physical parameterizations for

26   research and operational use. The system allows for feedback processes among gases, aerosol particles and

27   radiation, and includes a gas-phase module to simulate tropospheric gas-phase chemistry (Badia et al., 2016;

28   Jorba et al., 2012).

29   Its meteorological core, the Non-hydrostatic Multiscale Model on a B grid (NMMB), is a fully compressible

30   meteorological model with a non-hydrostatic option that allows for nested global-regional atmospheric

31   simulations by using consistent physics and dynamics formulations. The standard physical and numerical

32   schemes employed in NMMB are summarized in Table 1. The non-hydrostatic dynamics were designed to avoid

33   over-specification. The cost of the extra non-hydrostatic dynamics is about 20% of the cost of the hydrostatic

34   part, both in terms of computer time and memory (Janjic, 2001, 2003). The numerical schemes for the

35   hydrostatic and nonhydrostatic options available in the NMMB dynamic solver were designed following the

36   principles found in Janjic (1977) and developed and modified thereafter (Janjic, 1979, 1984, 2003) and are

37   summarized in Janjic and Gall (2012). The Arakawa B-grid horizontal staggering is applied in the horizontal

38   coordinate employing a rotated latitude-longitude coordinate for regional domains and latitude-longitude

Atmospheric
Chemistry
and Physics
Discussions

Open Access

1   coordinate with polar filtering for global domains. In the vertical, the Lorenz staggering vertical grid is used with

2   a hybrid sigma-pressure coordinate. The general time integration philosophy in NMMB uses explicit schemes

3   when possible for accuracy, computational efficiency and coding transparency (e.g., horizontal advection), and

4   implicit for very fast processes that would otherwise require a restrictively short time-step for numerical stability

5   with explicit differencing (e.g., vertical advection and diffusion, vertically propagating sound waves). The

6   NMMB model became the North American Mesoscale (NAM) operational meteorological model in October of

7   2011, and it has been computationally robust, efficient and reliable in operational applications and pre-

8   operational tests since then. In high-resolution NWP applications, the efficiency of the model significantly

9   exceeds those of several established state-of-the-art non-hydrostatic models (e.g. Janjic and Gall, 2012).

10

11   **3**   **The volcanic ash module: BSC-ASH**

12   The BSC-ASH module is embedded within the NMMB meteorological model and solves the mass balance

13   equation for volcanic ash taking into account: i) the characterization of the source term (emissions); ii) the

14   transport of volcanic particles (advection/diffusion); and iii) the particle removal mechanisms

15   (sedimentation/deposition). The coupling strategy of BSC-ASH can be turned on or off, depending on the

16   solution required (on-line vs. off-line). While the on-line version of the model offers a more realistic

17   representation of the meteorological conditions, the off-line approach uses an "effective wind fields", which

18   aims to replicate the decoupling effect of off-line dispersal models, for which the wind velocity and mid-layer

19   pressure (sigma) are set to constant during a given coupling interval. The conservativeness of the model is

20   evaluated to ensure that the ash transport scheme is consistent with the mass conservation equation.

21   **3.1**   **Source term**

22   Explosive volcanic eruptions release large amounts of particles into the atmosphere. These particles, commonly

23   known as tephra, mix with ambient air to form an eruption column or volcanic plume. To forecast the ash cloud

24   movement and provide actual ashfall concentrations, tephra dispersal models require a complete characterization

25   of the parameters describing the source term. These parameters are generally referred to as Eruption Source

26   Parameters (ESPs) and include the eruption start and duration, column height, mass eruption rate (MER), vertical

27   distribution of mass and the particle grain size distribution (GSD). ESPs vary not only from one eruption to

28   another, but also during the different eruptive phases of a single event.

29   Typically, the eruption starting time, duration and column height are inferred/constrained from visual or satellite

30   observations. However, other parameters such GSD, MER, or the vertical distribution of mass in the column are

31   not available in real-time and must be inferred from previous events of similar characteristics (e.g. Mastin et al.,

32   2009). Uncertainties in source parameter values are a key factor limiting the accuracy of ash-cloud model

33   forecasts (Bonadonna et al., 2015a). The characterization of each ESP in NMMB/BSC-ASH is described in the

34   following subsections.

Atmospheric
Chemistry
and Physics
Discussions

Open Access

1   **3.1.1   Mass eruption rate**

2   The Mass Eruption Rate (MER) gives the mass released by unit of time and defines the eruption intensity. Its

3   characterization in NMMB/BSC-ASH is achieved by employing a series of empirical correlations between

4   (observed) column height and eruption rate, which, according to plume similarity theory, scales roughly as the

5   4th power of height. Because of this strong dependence, uncertainties within 20% in the determination of column

6   height can translate into uncertainties up to 70% for the MER (e.g., Biass and Bonadonna, 2011). Averaged

7   column heights of eruptions that have not been directly observed are typically derived from characteristics of

8   tephra deposits (e.g. Bonadonna and Costa, 2013; Carey and Sparks, 1986; Pyle, 1989), or derived from model

9   inversion (e.g. Connor and Connor, 2006; Pfeiffer et al., 2005).

10   The empirical correlations to estimate MER in the model are described in Table 2, and are based either on fitting

11   observations (e.g. Mastin et al., 2009), or more sophisticated fits accounting for wind bent-over effects (e.g.

12   Degruyter and Bonadonna, 2012; Woodhouse et al., 2013). In addition, MER can also be derived using a more

13   sophisticated 1-D plume model (see Sect. 3.1.5).

14   **3.1.2   Vertical distribution of mass**

15   The vertical distribution of the initial column shape at the vent location is key when representing the plume,

16   especially if wind shear exists with elevation at the volcano (Lin, 2012). To determine the vertical distribution of

17   mass along the eruptive column, NMMB/BSC-ASH allows for the following geometrical distributions: i) point

18   source, where mass is released as a single source point at height, H_{plume}; ii) top-hat, where mass is released

19   along a umbrella-type slab of user-defined thickness, and iii) the so-called Suzuki distribution (Suzuki, 1983;

20   Pfeiffer et al., 2005), which assumes a more complex vertical distribution of mass release along the eruption

21   column;

22

$$S(z) = MER \left\{ \left(1 - \frac{z}{H_{plume}} \right) \exp \left[A \left(\frac{z}{H_{plume}} - 1 \right) \right] \right\}^{\lambda}$$

(4)

23   where, S is the mass per unit of time released at a given height z above the vent, MER is the total mass eruption

24   rate, H_{plume} is the column height, A and λ are the so-called Suzuki parameters. The parameter A dictates the

25   height of the maximum particle release (concentration), whereas λ controls how closely mass distributes around

26   this maximum. Any of the 3 options above can be combined independently with the different options for MER

27   estimation. In NMMB/BSC-ASH, the terrain following hybrid sigma-pressure vertical levels of the model must

28   be converted to elevations for each model integration time-step in order to interpolate MER from the discrete

29   source points into the nodes of the model grid.

30   **3.1.3   Grain size distribution**

31   The impact of explosive volcanic eruptions on climate and air traffic strongly depends on the concentration and

32   grain size distribution (GSD) of pyroclastic fragments injected into the atmosphere (e.g. Girault et al., 2014).

1 Grain size distribution is normally reconstructed by volcanologists from grain size data at individual outcrops,

2 ranging from basic unweighted average of the GSD at individual sparse outcrops, to various integration methods

3 of grain size data (e.g. Rose and Durant, 2009). The particle grain size distribution in NMMB/BSC-ASH is

4 specified through an input file, which defines the particle bin properties (bin mass fraction, diameter, density and

5 shape factor). As typical in volcanology, grain size distributions are given in terms of the Φ-number, defined as

6 $d = 2^{-\Phi}$, where d is the particle diameter in mm. The granulometry file in the model can be furnished by the

7 user (typically derived from field data) or generated by an external utility program which produces Gaussian and

8 Bi-Gaussian distributions in Φ (log-normal in diameter d) (Costa et al., 2016; Folch et al., 2009).

9 ### 3.1.4   Particle aggregation

10 The total grain size distribution (TGSD) erupted at the vent can be altered in case of particle aggregation, which

11 dramatically impacts particle transport dynamics thereby reducing the atmospheric residence time of aggregating

12 particles and promoting the premature fallout of fine ash. For computational purposes, particle aggregation in

13 NMMB/BSC-ASH is assumed to take place mainly in the eruption column, where particle concentration and

14 water contents are higher (the subsequent formation of aggregates downstream in the ash cloud under the

15 appropriate atmospheric conditions is not contemplated by the model). The model considers aggregates as

16 another particle class (bin), introduced as a standard source term by either solving: i) a series of simple analytical

17 expressions based on field observations or, ii) a more sophisticated wet aggregation model originally proposed

18 by Costa et al. (2010).

19 The analytical expressions available in the model modify the user-given particle grain size distribution by

20 assuming that a certain mass fraction of each granulometric class forms a new aggregate class added to the

21 TGSD. Despite the obvious limitations (obviates the physics of aggregation processes), these field-based

22 simplistic approaches are advantageous in that only the source term has to be modified in order to account for

23 aggregation. Table 3 provides an overview of these options. In addition to these empirical aggregation schemes,

24 NMMB/BSC-ASH also includes the wet aggregation model originally proposed by Costa et al. (2010). This

25 option allows for wet aggregation in the column providing an intermediate solution between the unaffordable all-

26 size class approach and the empirical solutions presented before. The model is based on a solution of the

27 classical Smoluchowski equation, obtained by introducing a similarity variable and a fractal relationship for the

28 number of primary particles in an aggregate. It also considers three different mechanisms for particle collision:

29 Brownian motion, ambient fluid shear, and differential sedimentation. Table 4 provides an overview of the

30 governing equations of this wet aggregation model.

31 ### 3.1.5   FPlume model

32 A more sophisticated approach to obtain MER and the mass distribution in the column from the conditions at the

33 vent consists of solving a 1-D radially averaged BPT model for mass, momentum, and energy. These 1-D plume

34 models are more useful in operational roles and broad exploratory investigations (Costa et al., 2015; Devenish et

35 al., 2012). For that reason, NMMB/BSC-ASH is coupled with the 1-D FPlume model (Folch et al., 2015); a 1-D

36 cross-section averaged plume model which accounts for plume bent over, entrainment of ambient moisture,

37 effects of water phase changes on the energy budget, particle fallout and re-entrainment by turbulent eddies, as

1   well as variable entrainment coefficients fitted from experiments. The model also accounts for particle

2   aggregation in presence of liquid water or ice that depends on column dynamics, particle properties, and amount

3   of liquid water and ice existing in the column (Folch et al., 2010). This allows the plume model to predict an

4   "effective" grain size distribution depleted in fines with respect to that erupted at the vent. For a complete

5   definition of the governing equations of FPlume, refer to Folch et al. (2015). FPlume has two solving strategies

6   where the model: i) solves directly for column height for a given MER; or ii) solves iteratively for MER for a

7   given height. For any case, the following inputs need to be provided to the ash input file in NMMB/BSC-ASH:

8   eruption start and duration, vent coordinates and elevation, conditions at the vent (exit velocity, temperature,

9   magmatic water mass fraction, and total grain size distribution) and total column height or mass eruption rate.

10   **3.2   Particle advection/diffusion**

11   Transport of volcanic ash by advection and turbulent diffusion is analogous to those of atmospheric tracers (e.g.

12   moisture) transport (Janjic et al., 2009) in NMMB. Tracer advection is Eulerian, positive-definite and

13   monotonic. The Adams-Bashforth scheme is used for horizontal advection and the Crank-Nicholson scheme for

14   vertical advection. For the horizontal diffusion, the model uses a second order scheme with two types of

15   parameterized dissipative processes: explicit lateral diffusion (often called horizontal diffusion, a 2nd order

16   nonlinear Smagorinsky-type approach; Janjic, 1990) and horizontal divergence damping (Janjic and Gall, 2012).

17   Plumes from high-intensity eruptions can be injected high into the stratosphere, reaching a maximum column

18   height and intruding laterally at the neutral buoyancy level (NBL) as a gravity current (Sparks et al., 1997). This

19   current can spread at velocities exceeding those of the surrounding winds, affecting tephra transport and

20   deposition near the source. As larger particles are removed by deposition and air is entrained, the plume density

21   decreases and momentum reduces such that, at a certain distance, atmospheric turbulence and wind advection

22   become the dominant atmospheric transport mechanisms (Baines and Sparks, 2005). Neglecting the gravitational

23   spreading of the umbrella cloud in tephra dispersal simulations could misrepresent the interaction of the volcanic

24   ash cloud and the atmospheric wind field for high-intensity eruptions and for proximal deposition of tephra

25   (Mastin et al., 2014). To account for the gravity-driven transport, NMMB/BSC-ASH is coupled with the model

26   of Costa et al. (2013) describing cloud spreading as a gravity current. This parameterization calculates an

27   effective radial velocity of the umbrella spreading as a function of time or cloud radius. The effective radial

28   velocity of the umbrella spreading is then combined with the wind field velocity centered above the vent in the

29   umbrella region to calculate the contribution of the gravitational spreading to the total cloud spreading. To

30   estimate the radial distance at which the critical transition between gravity-driven and passive transport occurs,

31   the umbrella front velocity is compared with the mean wind velocity at the NBL estimating the Richardson

32   number. Table 5 provides an overview of the governing equations of the gravity current model embedded in

33   NMMB/BSC-ASH.

34   **3.3   Particle sedimentation and dry deposition**

35   Particle sedimentation in NMMB/BSC-ASH is governed by the terminal velocity of sedimenting particles. This

36   fall velocity is sensitive to particle size and atmospheric conditions, determining the residence time of ash

Atmospheric
Chemistry
and Physics
Discussions

Open Access

1   particles in the atmosphere. The NMMB/BSC-CTM model assumes that the settling velocities of aerosols

2   (mineral dust, sea salt, etc.) follow the Stokes law for spherical particles corrected by the Cunningham slip

3   factor. The Stokes law applies to the creeping or Stokes flow regime, in which the drag force is proportional to

4   particle velocity, and holds only for Reynolds numbers Re≤0.1. This method is considered an efficient removal

5   mechanism for small particles (< 20 µm). Therefore, calculated fallout times based on settling according to

6   Stokes Law are inaccurate for coarse ash (> 64 µm), which sediments much faster. In addition, ash particles are

7   not spherical, which complicates and further slows fallout. In order to simulate a wider spectrum of particle

8   sizes, NMMB/BSC-ASH adds a new sedimentation module that covers the turbulent regime (Re≥1000) in where

9   the drag force is proportional to the square of the particle velocity. In this case, the particle settling velocity, v_s,

10   can be expressed as:

11

$$v_s = \sqrt{\frac{4g\left(\rho_p - \rho_a\right)d}{3C_d\rho_a}}$$

(13)

12   where, ρ_a and ρ_p denote air and particle density, respectively, d is the particle equivalent diameter, and C_d is the

13   drag coefficient (depending on the Reynolds number). Strictly, the expression above is valid for spherical

14   particles in the turbulent regime but it is often generalized to the whole range of Re numbers and particle shapes

15   by defining the drag coefficient properly. Table 6 provides an overview of the different settling velocity models

16   available in NMMB/BSC-ASH, each relaying on different empirical evaluations of drag coefficient.

17   Dry deposition, acting at the bottom layer of the model, is a complex process depending on physical and

18   chemical properties of the particle, the underlying surface characteristics and micro-meteorological conditions.

19   Dry deposition in NMMB/BSC-ASH is based on that originally proposed by Zhang et al. (2001). This

20   parameterization has been updated to account for the different settling velocities available for volcanic particles -

21   Eq. (13). The dry deposition velocity in the model, v_d, is given by:

22

$$v_d = v_s + \frac{1}{(R_a - R_s)}$$

(18)

23   where, R_a is the aerodynamic resistance of the particle, and R_s is the surface resistance. It is worth mentioning

24   that, for most of its resident time, airborne volcanic ash lies above the near-surface atmospheric layers, where

25   gravitation dominates, implying that, in most cases, dry deposition has little influence on model results.

26   **3.4   Mass conservation**

27   Mass conservation is a critical requirement for any atmospheric transport algorithm. Non-conservative schemes

28   can significantly underestimate or overestimate concentrations, especially for long time integrations, in which it

Atmospheric
Chemistry
and Physics
Discussions

Open Access

1   is critical that the tracer advection scheme is consistent with the mass continuity equation (Jöckel et al., 2001).

2   Most mesoscale meteorological models use observation/analyzed fields or global model results as initial

3   conditions, and therefore they are not very sensitive to slowly accumulated mass inconsistencies as re-

4   initializations remove accumulations. However, dispersal models are usually very sensitive to mass

5   inconsistencies set in previous simulations or spin-up fields as initial conditions, thereby accumulating mass

6   inconsistencies. In addition to mass conservation, monotonicity and prevention of non-physical under and

7   overshoots in the solution are also a highly desirable characteristics in transport schemes (Rood, 1987). For these

8   reasons, the model includes a conservative, positive definite and monotone Eulerian scheme for advection. The

9   positive definiteness in the model is guaranteed by advecting the square root of the tracer using a modified

10   Adams-Bashforth scheme for the horizontal direction and a Crank-Nicholson scheme for the vertical direction.

11   The conservation of the tracer is achieved as a result of the conservation of quadratic quantities by the advection

12   scheme. Monotonization is applied *a posteriori* to eliminate new extrema (Janjic et al., 2009). The conservative

13   nature of NMMB/BSC-ASH is evaluated by calculating the mass flux at the boundaries (for regional domains)

14   of the computational domain, the airborne mass, and the mass deposited on the ground to verify mass

15   conservation at each time-step (e.g. < 0.5% mass creation for a 30 day simulation).

16   ### 3.5   Numerical performance

17   The high computational efficiency of the NMMB meteorological driver allows for the application of

18   nonhydrostatic dynamics at a global scale (Janjic et al., 2009), and supports that the NMMB/BSC-ASH could be

19   used in an operational forecast of volcanic ash clouds. Model parallelization is based on the well-established

20   Message Passing Interface (MPI) library. The computational domain is decomposed into sub-domains of nearly

21   equal size in order to balance the computational load, where each processor is in charge to solve the model

22   equations in one sub-domain. The Eulerian schemes in the model require relatively narrow and constant width

23   halos, which simplify and reduce communications.

24   To measure the time-to-solution required, we compute the parallel speed-up (computation speed) of the model;

25   that is, the performance gains of parallel processing in comparison to serial processing:

26

$$S_{(P)} = \frac{t_{(P=1)}}{t_{(P)}} \tag{19}$$

27

28   where S is the computed speed-up value, and t is the simulation run-time employing P processors instead of

29   running it serially ($P = 1$).

30   To evaluate the efficiency of the model while using the computational resources, the parallel efficiency of the

31   model is computed by looking at the ratio between the parallel speed-up over P:

32

$$E_{(P)} = \frac{S_{(P)}}{P} \tag{20}$$

Atmospheric
Chemistry
and Physics
Discussions

1

2   Parallel efficiency is used as a metric to determine how far the model's speed-up is from the ideal. If the speed-

3   up is ideal, the efficiency is 1, regardless of how many cores the program is running on. If the speed-up is less

4   than ideal, the efficiency is less than 1.

5

6   **4   Simulations and validation**

7   The forecast skills of NMMB/BSC-ASH have been tested for several well-characterized eruptions, including the

8   Pinatubo 1991 (Philippines), Etna 2001 (Italy), Chaitén 2008 (Chile) or Cordón Caulle 2011 (Chile) eruptions.

9   Here, we present two applications of the model for the ash dispersal forecast of weak and strong long lasting

10   eruptions. Section 4.1 summarizes the results of the regional and global simulations for the first days of the 2011

11   Cordón Caulle eruption. This event represents a suitable case study of strong long-lasting eruptions, which is

12   useful when evaluating the on-line coupling strategy of the model. In a parallel effort, Sect. 4.2 summarizes the

13   results from the regional configuration of the model for the 2001 Etna eruption. This eruption is a good example

14   of weak long-lasting eruptions, useful when evaluating the sedimentation mechanisms of the model against well-

15   characterized tephra deposits.

16   **4.1   The 2011 Cordón Caulle eruption**

17   The 2011 Cordón Caulle eruption was a typical mid-latitude Central and South Andean eruption, where

18   dominating winds carried ash clouds over the Andes causing abundant ash fallout across the Argentine

19   Patagonia. Besides the significant regional impacts on agriculture, livestock and water distribution systems, this

20   eruption stranded thousands of passengers due to air traffic disruptions in the southern hemisphere, thereby

21   causing important economic losses to airlines and society (e.g. Raga et al., 2013; Wilson et al., 2013). This event

22   is evidence of the global nature of the volcanic ash dispersion phenomena and highlights the need for accurate

23   real-time forecasts of ash clouds.

24   The Cordón Caulle volcanic complex (Chile, 40.5º S, 72.2º W, vent height 1420 m a.s.l.) reawakened on 4 June

25   2011 around 18:30 UTC after decades of quiescence. The initial explosive phase spanned over more than two

26   weeks, generating ash clouds that dispersed over the Andes. The climatic phase (~27 h) (Jay et al., 2014) was

27   associated with a ~9 km (a.s.l.) high column (Osores et al., 2014). For the period between 4 - 14 June, numerous

28   flights were disrupted in Paraguay, Uruguay, Chile, southern Argentina and Brazil. The two major airports

29   serving Buenos Aires and the international airport in Montevideo, Uruguay, were closed for several days, along

30   with airports in Patagonia (Wilson et al., 2013). A detailed chronology of the eruption can be found in Collini et

31   al. (2013), the stratigraphy and characteristics of the resulting fallout deposit are described in Pistolesi et al.

32   (2015) and Bonadonna et al., (2015b), and a summary of the environmental impacts of the eruption is discussed

33   in Raga et al. (2013) and Wilson et al. (2013).

34   Figure 2 shows the synoptic meteorological situation during the 6-16 June. Here, we give a brief chronology of

35   the events that occurred during the first two weeks of eruptive activity in order to compare them with the

36   predictions of the model. In particular, we focus on the three major dispersion episodes occurring between the 6 -

Atmospheric
Chemistry
and Physics
Discussions

Open Access

EGU

1   8 June. The first major episode, on 6 June, resulted in a cloud moving northwards at high atmospheric pressure

2   (300 hPa), reaching the northern regions of the Argentine Patagonia threating the Buenos Aires air space. This

3   resulted in major air traffic disruption at the two international airports that service the city: Aeroparque (AEP)

4   and Ezeiza (EZE), which remained closed intermittently during the following 15 days. A complementary episode

5   dispersed ash further to the north of Argentina leading to a more recognizable shift of winds over the E-SE. In

6   the morning of 7 June, the initial trough reached the northern boundary of Paraguay coinciding with fallout of

7   snow and rain over Patagonia. Later during the day, the wind turned SE dispersing ash over Uruguay, Brazil and

8   Paraguay. During 8 and 9 June, the trough intensified, shifting the ash dispersion NE throughout the trough-ridge

9   structure. During the first hours of 9 June, the ash cloud reached the city of Buenos Aires following a frontal

10 zone passing through Patagonia, leaving a thin ash layer across the area. Ash cloud continued to change in

11 direction over the next 6 days, with clouds following the ridge structure to the NE and SE, respectively.

12 Afterwards, the cloud travelled S–SE, affecting the southern part of the Patagonia and Chile.

13 **4.1.1.   Regional simulation**

14 *Model set-up*

15 The model domain for the regional run is presented in Table 7 and consists of 268x268 grid points covering the

16 northern regions of Chile and Argentina using a rotated latitude–longitude grid with a horizontal resolution of

17 0.15º x 0.15º and 60 vertical layers. The top pressure of the model was set to 21 hPa (∼34 km) with a mesh

18 refinement near the top (to capture the dispersion of ash) and the ground (to capture the characteristics of the

19 atmospheric boundary layer). The computational domain spans in longitude from 41º W to 81º W and in latitude

20 from 18º S to 58º S. Runs were performed with the on-line version of NMMB/BSC-ASH from 3 June 2011 at

21 00:00 UTC to 21 June 2011 at 00:00 UTC. The integration time-step for the meteorological core and aerosol

22 transport was set to 30 seconds. The dynamic time-steps for the long and short wave radiations were computed

23 every 120 time-steps. Feedback effects of ash particles on meteorology and radiation were not included in this

24 run. The meteorological driver was initialized with wind fields from the Era-Interim reanalysis at 0.75º x 0.75º

25 resolution as initial and 6-h boundary conditions. In order to reduce the errors in meteorological conditions, they

26 were reinitialized every 24 h with a spin-up of 12 h. Daily eruption source parameters (ESP) were obtained from

27 Osores et al. (2014), who estimated column heights for each eruptive pulse using the Imager Sensor data from

28 the GOES-13 satellite. Mass flow rate released along the column was derived from column heights based on

29 Mastin et al. (2009), assuming a Suzuki vertical distribution of mass typical of explosive Plinian eruptions (A=4 ;

30 λ=5). Grain size distribution was obtained from Collini et al. (2013) and discretized in 10 bins ranging from -1Φ

31 (2 mm) to 8Φ (4 μm) with a linear dependency of particle density on diameter ranging from 1.000 to 2.200 kg m⁻

32 ³. Particle sphericity was set to a constant standard value of 0.9 for all bins. The *percentage* aggregation model

33 was used to update the TGSD with a new bin for aggregates, resulting in a total of 11 bins.

34 *Validation of results against satellite imagery*

35 Model results for the airborne mass concentration of ash were validated using qualitative and quantitative

36 comparisons with data obtained using two different techniques. On one end, we performed a qualitative

37 comparison between the simulated column mass (g m⁻²) from the model and the NOAA-AVHRR satellite

1   imagery provided by the high-resolution picture transmission (HRPT) division of the Argentinian National

2   Meteorological Service. Figure 3 shows how the NMMB/BSC-ASH predictions for cloud trajectory and arrival

3   times are in agreement with observations, capturing the three major dispersion episodes. It should be noted that

4   these types of images are not directly comparable because the MODIS ash detection threshold and the

5   reflectivity coefficients of volcanic ash are not well constrained. However, the figure illustrates the capability of

6   the model to predict the variation of the cloud position with time.

7   Column mass simulations were also validated against ash mass loadings presented by (Osores et al., 2015), who

8   retrieved ash-contaminated pixels detected on the basis of the concept of reverse absorption (Prata, 1989a,

9   1989b), i.e. those pixels with brightness temperature differences between 11 and 12 μm (BTD11-12 μm) that are

10   lower than 0.0 K. To minimize the presence of false positives, pixels with a BTD11-12 μm > -0.6 K and clear

11   sky pixels were removed. Mass loadings were mapped up to 15 g m^{-2} based on an approach which combines the

12   satellite data with look-up tables of brightness temperatures obtained with a radiative transfer model and optical

13   properties of andesite volcanic rocks (Prata, 2011). Figure 4 shows a good quantitative agreement between the

14   model results and the airborne ash mass loadings described above.

15   *Validation of results against fallout deposit*

16   Tephra was mostly deposited eastward from the source during the first 72 h of the event within an elongated area

17   between 40-42º S and 64-72º W. Results from the NMMB/BSC-ASH forecast for ash deposition were validated

18   against: i) a detailed characterization of the proximal deposit for the first 72 h of the eruption, and ii) an isopach

19   map derived from measurements taken for the period beginning on 4 June until 30 June (Collini et al., 2013).

20   To evaluate the simulated computed thicknesses (cm) by the model near the vent during the first 72 h of the

21   event, model results were compared against a comprehensive classification of the proximal deposit presented by

22   Pistolesi et al. (2015b), who constrained the stratigraphic sequence of the deposit in different Units (phases).

23   Here, we constrain the deposit to the first three units of their work, corresponding to the first 72 h of the eruptive

24   even and including: i) Unit I, containing coarser-grained layers A-B, representing the very first stage of the

25   eruption within the first 50 km from the vent, and layers A–F associated to the first 24-30 h of the eruption

26   (afternoon of 4 to morning of 5 June); ii) Unit II, containing layer H, a fine pumice lapilli layer which was

27   emplaced starting on the night of 6 June; iii) Unit III, enclosing layer K2, the easiest to identify from several

28   coarser (fine-lapilli) grain-size layers, and being associated to the morning of 7 June. Figure 5 shows that

29   NMMB/BSC-ASH can reproduce the deposit presented by Pistolesi et al. (2015b) both in time and space. Key

30   sections located along the dispersal area (e.g. San Carlos de Bariloche – SCB, 90 km from the vent; Ingeniero

31   Jacobacci – IJ, 240 km east of the vent) were used as geographic references.

32   To evaluate the model performance at the end of our simulation, model results were also validated against an

33   isopach map derived from measurements taken from the 4 to 30 June presented by Collini et al. (2013). Deposit

34   load variations produced by remobilization were not considered in this analysis. Figure 6 shows good agreement

35   between the modeled deposit load (kg m^{-2}) at the end of the simulation and the measured ground deposit

36   isopachs (kg m^{-2}) at 30 June from Collini et al. (2013).

Atmospheric
Chemistry
and Physics
Discussions

1   The model resulted in a cumulative mass of $\sim 4.2 \times 10^{11}$ kg. This value is in agreement with previous works,

2   where total mass was either modeled (Collini et al., 2013) or estimated by empirical fits (Bonadonna et al.,

3   2015b). Ashfall forecast with the NMMB/BSC-ASH model represented well the overall deposit load for the

4   2011 Caulle eruption.

5   **4.1.2   Global simulation**

6   For this simulation, the global domain was configured using a regular latitude–longitude grid with a horizontal

7   resolution of 0.75º × 1º and 60 vertical layers. The ash distribution is simulated between 3-21 June 2011 using

8   the Era-Interim reanalysis at 0.75º x 0.75º resolution as initial and 6-h boundary conditions. Meteorological

9   conditions for the global runs were also reinizialized every 24h. The atmospheric model's fundamental time-

10 step was set to 180 s, while the rest of the model variables remained the same as in the regional simulation.

11 Figure 7 shows the global dispersal of ash for the 2011 Cordon Caulle eruption after different times of the

12 simulation. As it can be inferred from this figure, by 10 June, the plume entered the Australian and New Zealand

13 airspace (Fig 7b) covering more than half of the southern hemisphere. At that point, the Civil Aviation Authority

14 of New Zealand warned pilots that the ash cloud was between 20,000 and 35,000 feet (6 to 11 kilometers), the

15 average cruising level for many aircraft (Sommer, 2011). Before the end of our simulation, on 13 June the ash

16 cloud had completed its first circle around the globe. This is in agreement to satellite images reported by the

17 Darwin Volcanic Ash Advisory Centre (Darwin VAAC, 2011). Finally, results from the global simulation are

18 also in agreement with those from our regional run.

19 **4.1.3   Forecasting impacts on civil aviation**

20 NMMB/BSC-ASH can furnish values of airborne concentration at relevant flight levels (FL), defined as the

21 vertical altitude (expressed in hundred of feet) at standard pressure at which the ash concentration is measured.

22 This information is particularly important for air traffic management and can be used to decide alternative routes

23 to avoid an encounter with a volcanic cloud. Airborne concentration at FL050 (5,000 feet on nominal pressure) is

24 relevant for the determination of flight cancellations and airports closure, while concentrations at FL300 (30,000

25 feet) are critical to assist flight dispatchers while planning flight paths and designing alternative routes in the

26 presence of a volcanic eruption. The model runs as if responding to an eruptive event, i.e. we only used the semi-

27 quantitative data available at that time as volcanological inputs.

28 Figure 8 shows the airspace contamination forecasted by NMMB/BSC-ASH during the 6-7 June at flight levels

29 FL050 and FL300, within a latitude band between 20º S and 55º S. Model results show the volcanic cloud

30 twisting in different directions during that period of time, achieving critical concentration values within a wide

31 area east of the Andes range. On 6 June, simulation results show the volcanic cloud at high atmospheric pressure

32 (~ 30,000 feet or 300 hPa) moving northwards, and the one at lower atmospheric pressure (~ 5,000 ft or 50 hPa)

33 threatening the main international airports that service the region of Buenos Aires (Fig. 8a). In the morning of 7

34 June, the ash cloud present at lower atmospheric pressure (~ 5,000 ft or 50 hPa) changed its direction towards the

35 SW, ultimately affecting part of the Patagonia and Chile (Fig. 8b), while higher ash clouds started their course

36 around the globe (Fig. 8c). These results suggest that the cancellation of multiple flights in several Argentinean

37 airports during this time was justified. It is important to point out that, for this work, our objective is not to

Atmospheric
Chemistry
and Physics
Discussions

1   perform a detailed study of the Caulle eruption but to use it as a blind test to confront short-term model

2   predictions and semi-quantitative syn-eruptive observations.

3   **4.2   The 2001 Mt. Etna eruption**

4   Mt. Etna is the most active volcano in Europe and constitutes a continuous hazard for eastern Sicily. Since 1980,

5   Mt. Etna has injected large volumes of pyroclasts into the atmosphere (between 10^4 and 10^7 m^3 per event) over

6   more than 160 eruptive episodes (Scollo et al., 2012). The explosive activity of Mt. Etna reached its climax in

7   2001 and 2002–03 when two major flank eruptions occurred; both characterized by long-lasting explosive

8   activity (Branca and Del Carlo, 2005). The 2001 event represents a good case to evaluate the deposition

9   mechanisms of NMMB/BSC-ASH against the well-characterized tephra deposit reported in Scollo et al. (2007).

10   The explosive activity at the 2570 m vent had three main phases characterized by phreatomagmatic, magmatic

11   and vulcanian explosions. The eruption started with a series of phreatomagmatic explosions during the first days

12   of the eruption. These explosions were followed by a second eruptive phase characterized by strombolian and

13   Hawaiian style explosions during 19-24 July. The explosive activity continued until 6 August with a series of

14   vulcanian explosions. Tephra fallout associated to the explosive activity during 21-24 July represented a major

15   source of hazard for eastern Sicily. Flight operations were cancelled at the Catania and Reggio Calabria airports

16   during the 22 and 23 July (Scollo et al., 2007). A detailed chronology of the eruption can be found in Scollo et

17   al. (2007). Volcanic plumes were captured by the Multiangle Imaging Spectro Radiometer (MISR) on board

18   NASA's Terra spacecraft, and analyzed with stereo matching techniques to evaluate the height of the volcanic

19   aerosol with a precision of a few hundred meters (Scollo et al., 2012).

20   Here, we validate NMMB/BSC-ASH against the tephra deposit produced from the 2570 m vent for that period of

21   time, and compare the model performance against simulations results from the FALL3D model (Costa et al.,

22   2006; Folch et al., 2009) for the same event. FALL3D is an Eulerian model for transport and deposition of

23   volcanic ash particles solving a set of advection-diffusion-sedimentation equations (one equation for each

24   particle class) on a structured terrain following grid using a second-order Finite Differences explicit scheme. The

25   model is used at the Buenos Aires and Darwin Volcanic Ash Advisory Centers (VAAC) in operational forecasts.

26   **4.2.1   Regional simulation**

27   *Model set-up*

28   Two regional domains were used to simulate the first phase of the 2001 eruption of Mt. Etna (Table 8). The first

29   domain (Regional 1), used to reconstruct the tephra deposit, consists of 101x101 grid points covering the SE

30   flank using a rotated latitude–longitude grid with a horizontal resolution of 0.05º x 0.05º and 60 vertical layers.

31   Similarly to the Cordón Caulle simulations, the top pressure of the model was set to 21 hPa (~34 km) with a

32   mesh refinement near the top and ground. The computational domain spans in longitude from 12.5º E to 17.5º E,

33   in latitude from 35.25º N to 40.25º N. Simulation runs were performed with the on-line version of NMMB/BSC-

34   ASH from 21 July 2001 at 00:00 UTC to 25 July 2001 at 00:00 UTC. The integration time-step for the

35   meteorological core was set to 10 seconds. The meteorological driver was initialized with Era-Interim reanalysis

36   meteorological data at 0.75º x 0.75º resolution as initial and 6-h boundary conditions. A spin-up of 12 h was used

Atmospheric
Chemistry
and Physics
Discussions

1   to prepare the meteorological conditions for run. Each daily model run was reinitialized with the corresponding
2   reanalysis, the NMMB/BSC-ASH tracers' output from the previous day, and the associated eruption source
3   parameters. Meteorological conditions were reinitialized every 24 h. The grain size distribution and eruption
4   source parameters were obtained from Scollo et al. (2007), who assumed a Suzuki vertical mass distribution
5   located at the middle of the eruption column (A=2; λ=1), and employed the Mastin et al. (2009) empirical
6   relationship to characterize the MER and the Voronoi tessellation method to obtain the grain size distribution.
7   Finally, sensitivity analyses were performed against the different aggregation schemes available in the model. In
8   all cases, the TGSD was updated with a new bin for aggregates, resulting in a total of 8 bins.

9   A second regional domain (Regional 2) was used to evaluate tephra dispersal between 21 and 25 of July. In this
10 case, the domain consisted of 201x201 grid points covering a computational domain spanning in longitude from
11 41º E to 81º E, in latitude from 18º S to 58º S. This domain used a coarser horizontal resolution of 0.1º x 0.1º and
12 60 vertical layers. The integration time-step for the meteorological core was set to 30 seconds. The rest of model
13 set-up was kept the same as in the first regional domain (Regional 1).

14 *Validation of results against fallout deposit*

15 At the end of the second explosive phase, a continuous tephra layer covered Etna's flanks between Giarre and
16 Catania (from E to S). Ash deposition results from NMMB/BSC-ASH were validated against 47 samples
17 collected between 25 and 26 July from measured areas on flat open spaces, where the deposit did not show any
18 reworking. The computed tephra dispersal and deposition from NMMB/ABSC-ASH was able to reproduce the
19 bilobate shape of the real deposit with the two axes oriented toward Acireale and Acicastello towns. Figure 9
20 compares the simulated deposit load (kg m^{-2}) at the end of the run against the isopachs map derived from
21 measurements taken from the 21-24 July (Scollo et al., 2007). The model resulted in a cumulative mass of
22 $\sim 1.18 \times 10^9$ kg. This value is in agreement with the results obtained from Scollo et al. (2007).

23 **4.2.2   Model intercomparison: NMMB/BSC-ASH vs. FALL3D**

24 To validate the model performance of NMMB/BSC-ASH for its operational implementation, we compare the
25 tephra deposition results of the model against those of the operational FALL3D model for the reconstruction of
26 the 2001 Mt. Etna eruption. For this comparison we ran both models using the same meteorological and
27 volcanological initial conditions (Table 8). Figure 10 shows the simulated thicknesses (vertical axis) for both
28 transport models against the observations (horizontal axis) presented in Scollo et al. (2007. The model improved
29 the tephra distribution results from FALL3D simulations for the same event (R^2; 0.80/0.62), reducing the RMSE
30 (0.014/0.24) and bias (0.02/0.6) and the computational time by an order of magnitude. In particular, all values
31 simulated with NMMB/BSC-ASH plot inside the region between 5 and 1/5 (dashed orange line) times the
32 observed mass at each station. The greatest differences observed against the observations for both models belong
33 to those points located at distances less than 15 km from the vent associated to the uncertainty in the ESPs. The
34 mean value of the relative error between the computed values and observed data is 64%, which improves those
35 from FALL3d (91%), and are comparable with those of Scollo et al., (2007), who obtained a 57% by deposit
36 best-fitting using the HAZMAP dispersion model

37

Atmospheric
Chemistry
and Physics
Discussions

5   Operational forecast with NMMB/BSC-ASH

Employing on-line models for operational dispersal forecast requires larger computational resources and is not always feasible at all operational institutes. Nevertheless, due to the increase in computing power of modern systems, one can argue that such gradual migration towards stronger on-line coupling of NWPMs with TDMs poses a challenging but attractive perspective from the scientific point of view for the sake of both high-quality meteorological and volcanic ash forecasting. The focus on volcanic aerosols integrated systems in operational forecast is timely, since recent research has shown that meteorology and chemistry feedbacks are important in the context of many research areas and applications (e.g., NWP and air quality forecasting, climate and Earth system modeling (Baklanov et al., 2014)).

In that context, the Barcelona Supercomputing Center is currently working on a modeling integrated system to provide operational forecast of volcanic ash with NMMB/BSC-ASH. The system includes a preprocessing tool (prepares the model for real-data simulations), an executable file to run the model, and a user-based postprocessing utility tool. Figure 11 shows a simple schematic representation of the operational implementation of NMMB/BSC-ASH. The outcomes of this modeling system are currently being evaluated against two operational models: i) the NOAA/ARL Hybrid Single Particle Lagrangian Integrated Trajectory Model (HYSPLIT; Draxler and Hess, 1998) – used at the Washington VACC; and FALL3D (Costa et al., 2006; Folch et al., 2009) – used at the Buenos Aires and Darwin VAACs. This section introduces the structure of the operational NMMB/BSC-ASH system. Preliminary results for the model intercomparison against FALL3D are described in Sect. 4.2.2.

5.2   The preprocessing system

The preprocessing utility system consists of a set of programs whose collective role is to prepare the model for real-data simulations. Programs are grouped to preprocess geographical, meteorological and climatological inputs and interpolate them to the model grid(s). The preprocessing system uses three main programs: *runfix*, *degrib* and *runvariable*.

- *Runfix* defines the model domain(s) and interpolates static geographical data to the model grid(s). In addition to computing the latitude and longitude of the rotated grid points, this program interpolates soil categories, land use types, terrain height, annual mean deep soil temperature, monthly albedo, maximum snow albedo, and slope category.
- *Degrib* extracts the necessary meteorological fields from GRIB-formatted files, used as initial condition for global simulations and as initial and boundary conditions for single regional domains (i.e. not nested with a global domain). GRIB files contain time-varying meteorological fields obtained from another regional or global NWPM. In addition to the available NCEP's North American Model (NAM) or Global Forecast System (GFS) model, the program has been updated to include European Centre for Medium-Range Weather Forecasts (ECMWF) ERA-Interim reanalysis data (Dee et al., 2011) as forcing.
- *Runvariable* interpolates the meteorological fields extracted by *debgrib* to the model grid(s) defined by *runfix* and prepares the climatological schemes. This program generates the initial and boundary

16

Atmospheric
Chemistry
and Physics
Discussions

1   conditions that are ingested by NMMB using the NOAA Environmental Modeling System (NEMS;

2   Janjic, 2005; Janjic and Black, 2007), a high performance software superstructure and infrastructure

3   based on the Earth System Modeling Framework (ESMF) for use in operational prediction models at

4   NCEP.

5   ### 5.3   BSC-ASH I/O files

6   The model takes three run-specific input files:

7   • The model input file (*nmmb.inp*), which defines the computational and physical schemes needed by the

8   meteorological core, the atmospheric model's fundamental time-step, and the parameterization for

9   chemical processes and radiative schemes for aerosol tracers (including ash), amongst other properties

10 of the model. For long-lasting eruptions, the model performs restart runs initializing the tracers from the

11 previous day's history file.

12 • The ash input file (*ash.inp*), which defines the source term. The user-defined parameters include the

13 eruption source type, column height and determination of the mass eruption rate, eruption duration,

14 gravity current conditions, aggregation processes, and particle settling velocity model. In the event of

15 various eruptive phases, the respective ESPs for each phase can be defined. Finally, the file also defines

16 the coupling strategy (on vs. off-line) employed by the model.

17 • The granulometry input file (*ash.tgsd*), which specifies the diameter, density, sphericity, and relative

18 mass fraction of each particle bin. This information is typically obtained from field data or created by

19 external utility programs for idealized grain size distributions. If aggregation is active, a new bin class

20 for aggregates is added to the granulometry input file.

21 Once a simulation is concluded, NMMB/BSC-ASH writes the following output files:

22 • A log file (*ash.log*), containing information about the run, including a summary of the computed

23 volcanic ash source and mass balance statistics for each time-step, and errors and warnings if any.

24 • A forecast results file (*problemname.nc*) in NetCDF format containing, amongst other variables, the

25 total column mass concentration ($g\ m^{-2}$) and ground deposition ($kg\ m^{-2}$) for all bins, the concentration at

26 different Flight Levels ($g\ m^{-3}$) and the Aerosol Optical Depth. This information can be processed using

27 several open-source programs to generate plots and animations. Alternatively, the post-process utility

28 program *NMMB2GMT* has been developed to generate basic GMT scripts automatically.

29 • A restart file (*nmmb.hst*) used to initiate a new run using the ash concentrations from a previous

30 simulation.

31 ### 5.4   The Postprocess system

32 The postprocess utility tools are designed to interpolate outputs from the NMMB/BSC-ASH native grid(s) to

33 National Weather Service (NWS) standard levels (pressure, height, etc.) and standard output grids (Lambert

34 Conformal, polar-stereographic, etc.) in NetCDF format. The system also includes the *NMMB2GMT* program,

35 which uses the Generic Mapping Tools (GMT) software (Wessel and Smith, 1991) to produce similar plots to

36 the Volcanic Ash Graphics (VAG) used by Volcanic Ash Advisory Centers in operational forecasts.

Atmospheric
Chemistry
and Physics
Discussions

1   **5.5   Scalability analysis**

2   To optimize a future operational implementation of the model, we aim to minimize the time-to-solution avoiding

3   communication overhead. In this context, we evaluate the model scalability (scaling efficiency) for its regional

4   and global configurations by performing a strong scalability test, in which the problem size of our simulation

5   (e.g., model domain and resolution) remains fixed while increasing the number of processing cores. Figure 12

6   shows the parallel speed-up (S; Eq. 19), and efficiency (E; Eq. 19) of the NMMB/BSC-ASH system for a global

7   simulation of the climatic phase for the 2011 Cordón Caulle (Table 7). On the MareNostrum-III supercomputer,

8   maximum efficiency for the global simulation described in Table 7 is reached at ≈ 32 nodes (16 CPUs each) with

9   a parallel efficiency of 0.6.

10   The scalability analysis was performed on all the available source term and sedimentation schemes in the model.

11   The relative computational cost associated with the main processes in NMMB/BSC-ASH is presented in Fig.

12   13. Processes represented include: meteorological prediction, volcanic ash transport and sedimentation forecast,

13   aggregation of particles, gravity current effects, and the restart phase. The restart phase represents the CPU time

14   employed to rerun the preprocess system every 24h of simulation. This figure suggests that the computational

15   increase (CPU time) associated to the ash module can vary from 5 to 55%, depending on the number of

16   computational nodes employed. It is important to note that, depending on the settling velocity model employed,

17   up to 60% of the time allocated to the ash module is assigned to the sedimentation term.

18   Results from the scalability analysis show that the model performance (in terms of speed-up) depends on the

19   problem size as well as on the domain partitioning topology. In that context, the relative computational cost of

20   the model's meteorological core (NMMB) is evaluated as a function of its domain decomposition (e.g.,

21   distribution of processing units for the horizontal domains – nodes i and j). For this analysis the bin-performance

22   dependency of the model is considered, therefore evaluating only the cost of one bin of ash. Results from this

23   analysis suggest that, for an optimal simulation using 32 nodes, the computational cost of the meteorological

24   core decreases over 10 % when the weight of the decomposition is focused on the j nodes (e.g., more

25   computational resources assigned for the Fast Fourier Transformation algorithm). The best domain

26   decomposition resulted in 6(i)x84(j)+8(w), being the number of writing processors.

27   For operational purposes, the computational time employed to provide ash dispersal forecast using NMMB/BSC-

28   ASH is evaluated for the global simulation with 1 bin of ash. The maximum time required by the model to

29   perform a 24 h forecast, running all the available processes (e.g., advection, diffusion, sedimentation, etc.) every

30   time-step (180 seconds) is less than 3 minutes when using the best domain decomposition presented before

31   (6x84+8). This time can be further optimized for operational purposes, i.e., calling the model physics less

32   frequently in order to save computational time. As a general rule of thumb, the adjustment time-step in seconds

33   for the meteorological core can be taken as 2.25 times the grid spacing in kilometers. For higher resolution

34   model runs made without parameterized convection, a time-step in seconds of about 1.9 to 2.0 times the grid

35   spacing may be more appropriate (Janjic and Gall, 2012).

36

1   **6   Summary and Conclusions**

2   We present NMMB/BSC-ASH, a new on-line multiscale meteorological and transport model developed at the

3   Barcelona Supercomputing Center (BSC) to forecast the dispersal and deposition of volcanic aerosols. The

4   objective of NMMB/BSC-ASH is to improve the current state-of-the-art of tephra dispersal models, especially in

5   situations where meteorological conditions are fluctuating rapidly in time, two-way feedbacks are significant, or

6   long-rage ash cloud dispersal predictions are necessary. The model predicts ash cloud trajectories, concentration

7   of ash at relevant flight levels, and the expected deposit thickness for both regional and global domains.

8   NMMB/BSC-ASH solves the mass balance equation for volcanic ash by means of a new ash module embedded

9   in the BSC's operational system for short/mid-term chemical weather forecasts (NMMB/BSC-CTM). In addition

10   to volcanic ash, the system is also capable to forecast the dispersion of other atmospheric aerosols (e.g. dust, sea

11   salt, black carbon, organic aerosol, sulfates, etc.). Its multiscale capability allows for nested global-regional

12   atmospheric transport simulations, taking into account the characterization of the source term (emissions), the

13   transport of volcanic particles (advection/diffusion), and the particle removal mechanisms

14   (sedimentation/deposition). The model has been shown to be robust and scalable to arbitrary domain sizes

15   (regional to global) and numbers of processors.

16   The forecast skills of NMMB/BSC-ASH have been validated against several well-characterized eruptions,

17   including the Pinatubo 1991 (Philippines), Etna 2001 (Italy), Chaitén 2008 (Chile) or Cordón Caulle 2011

18   (Chile) eruptions. To evaluate the on-line coupling strategy and the multiscale capability of the model, this paper

19   summarizes the regional and global configurations of the model to forecast the dispersal of ash for the first days

20   of the 2011 Cordón Caulle eruption (strong long-lasting eruption with rapid wind changes). In addition, to

21   evaluate the sedimentation mechanisms of the model, this work also includes the results from the regional

22   configuration of the model for the first phase of the 2001 Etna eruption, a good case study of weak long-lasting

23   eruption with well-characterized tephra deposits. Simulation results demonstrate that NMMB/BSC-ASH is

24   capable to reproduce the spatial and temporal dispersal variability of the ash cloud and tephra deposits.

25

26   **Software**

27   The work described in this paper is based on version 2.0.1 (released in April, 2014). The code, written in

28   FORTRAN-90, is portable and efficient on available parallel computing platforms. The figures presented in this

29   paper were generated using Gnuplot and NCAR Command Language (NCL).

30

31   **Acknowledgements**

Atmospheric
Chemistry
and Physics
Discussions

Open Access

1   MareNostrum Supercomputer using 512 and 256 - 8x4 GB DDR3-1600 DIMMS (2GB/core) Intel SandyBridge

2   processors, iDataPlex Compute Racks, a Linux Operating System and an Infiniband interconnection.

3

4   **Competing interests**

5   The authors declare that they have no conflict of interest.

6

Atmospheric
Chemistry
and Physics
Discussions

Open Access

EGU

1   **References**

2   Ames, W.: Numerical methods for partial differential equations, Nelson. London., 1969.

3   Arastoopour, H., Wang, C.-H. and Weil, S. A.: Particle-particle interaction force in a dilute gas-solid system,
4   Chem. Eng. Sci., 37(9), 1379–1386, doi:10.1016/0009-2509(82)85010-0, 1982.

5   Badia, A., Jorba, O., Voulgarakis, A., Dabdub, D., Pérez García-Pando, C., Hilboll, A., Gonçalves, M. and
6   Janjic, Z.: Gas-phase chemistry in the online multiscale NMMB/BSC Chemical Transport Model: Description
7   and evaluation at global scale, Geosci. Model Dev. Discuss., (2), 1–47, doi:10.5194/gmd-2016-141, 2016.

8   Baines, P. and Sparks, R. S. J.: Dynamics of giant volcanic ash clouds from supervolcanic eruptions, Geophys.
9   Res. Lett., 32(December), 1–4, doi:10.1029/2005GL024597, 2005.

10   Baklanov, A., Schlünzen, K., Suppan, P., Baldasano, J. M., Brunner, D., Aksoyoglu, S., Carmichael, G., Douros,
11   J., Flemming, J., Forkel, R., Galmarini, S., Gauss, M., Grell, G., Hirtl, M., Joffre, S., Jorba, O., Kaas, E., Kaasik,
12   M., Kallos, G., Kong, X., Korsholm, U., Kurganskiy, A., Kushta, J., Lohmann, U., Mahura, A., Manders-Groot,
13   A., Maurizi, A., Moussiopoulos, N., Rao, S. T., Savage, N., Seigneur, C., Sokhi, R. S., Solazzo, E., Solomos, S.,
14   Sørensen, B., Tsegas, G., Vignati, E., Vogel, B. and Zhang, Y.: Online coupled regional meteorology chemistry
15   models in Europe: Current status and prospects, Atmos. Chem. Phys., 14(November 2013), 317–398,
16   doi:10.5194/acp-14-317-2014, 2014.

17   Betts, A. K. and Miller, M. J.: A new convective adjustment scheme. Part II: Single column tests using GATE
18   wave, BOMEX, ATEX and arctic air-mass data sets, Q. J. R. Meteorol. Soc., 112(473), 693–709,
19   doi:10.1002/qj.49711247308, 1986.

20   Biass, S. and Bonadonna, C.: A quantitative uncertainty assessment of eruptive parameters derived from tephra
21   deposits: The example of two large eruptions of Cotopaxi volcano, Ecuador, Bull. Volcanol., 73(1), 73–90,
22   doi:10.1007/s00445-010-0404-5, 2011.

23   Bonadonna, C. and Costa, A.: Plume height, volume, and classification of explosive volcanic eruptions based on
24   the Weibull function, Bull. Volcanol., 75, 1–19, doi:10.1007/s00445-013-0742-1, 2013.

25   Bonadonna, C., Biass, S. and Costa, A.: Physical characterization of explosive volcanic eruptions based on
26   tephra deposits: Propagation of uncertainties and sensitivity analysis, J. Volcanol. Geotherm. Res.,
27   doi:10.1016/j.jvolgeores.2015.03.009, 2015a.

28   Bonadonna, C., Cioni, R. and Pistolesi, M.: Sedimentation of long-lasting wind-affected volcanic plumes : the
29   example of the 2011 rhyolitic Cordón Caulle eruption, Chile, Bull. Volcanol., doi:10.1007/s00445-015-0900-8,
30   2015b.

31   Branca, S. and Del Carlo, P.: Types of eruptions of Etna volcano AD 1670-2003: Implications for short-term
32   eruptive behaviour, Bull. Volcanol., 67(8), 732–742, doi:10.1007/s00445-005-0412-z, 2005.

33   Carey, S. and Sparks, R. S. J.: Quantitative models of the fallout and dispersal of tephra from volcanic eruption
34   columns, Bull. Volcanol., 48(2-3), 109–125, doi:10.1007/BF01046546, 1986.

35   Casadevall, T. J.: Volcanic Hazards and Aviation Safety : Lessons of the Past Decade., 1993.

Atmospheric
Chemistry
and Physics
Discussions

Open Access

Collini, E., Osores, M. S., Folch, A., Viramonte, J., Villarosa, G. and Salmuni, G.: Volcanic ash forecast during the June 2011 Cordón Caulle eruption, Nat. Hazards, 66, 389–412, doi:10.1007/s11069-012-0492-y, 2013.

Connor, L. and Connor, C.: Inversion is the Key to Dispersion : Understanding Eruption Dynamics by Inverting Tephra Fallout, Special Publications of IAVCEI, 1. Geological Society, London, pp. 231–242., 2006.

Cornell, W., Carey, S. and Sigurdsson, H.: Computer simulation of transport and deposition of the Campanian Y-5 ash, J. Volcanol. Geotherm. Res., 17, 89–109, 1983.

Costa, A., Macedonio, G. and Folch, A.: A three-dimensional Eulerian model for transport and deposition of volcanic ashes, Earth Planet. Sci. Lett., 241, 634–647, doi:10.1016/j.epsl.2005.11.019, 2006.

Costa, A., Folch, A. and MacEdonio, G.: A model for wet aggregation of ash particles in volcanic plumes and clouds: 1. Theoretical formulation, J. Geophys. Res. Solid Earth, 115, 1–14, doi:10.1029/2009JB007175, 2010.

Costa, A., Folch, A. and Macedonio, G.: Density-driven transport in the umbrella region of volcanic clouds : Implications for tephra dispersion models, Geophys. Res. Lett., 40(July), 4823–4827, doi:10.1002/grl.50942, 2013.

Costa, A., Suzuki, Y., Cerminara, M., Devenish, B. J., Esposti Ongaro, T., Herzog, M., Van Eaton, A., Denby, L., Bursik, M., De' Michieli Vitturi, M., Engwell, S., Neri, A., Barsotti, S., Folch, A., Macedonio, G., Girault, F., Carazzo, G., Tait, S., Kaminski, É., Mastin, L., Woodhouse, M., Phillips, J., Hogg, A., Degruyter, W. and Bonadonna, C.: Overview of the Results of the Eruption Column Model Intercomparison Exercise, J. Volcanol. Geotherm. Res., doi:10.1016/j.jvolgeores.2016.01.017, 2015.

Costa, A., Pioli, L. and Bonadonna, C.: Assessing tephra total grain-size distribution: Insights from field data analysis, Earth Planet. Sci. Lett., 443(September), 90–107, doi:10.1016/j.epsl.2016.02.040, 2016.

Darwin VAAC: Satellite image of path of the Cordon Caulle ash cloud around the southern hemisphere from 5-12 June 2011, Bur. Meteorol. [online] Available from: http://www.bom.gov.au/info/vaac/cordon_caulle.shtml, 2011.

Dee, D. P., Uppala, S. M., Simmons, a. J., Berrisford, P., Poli, P., Kobayashi, S., Andrae, U., Balmaseda, M. a., Balsamo, G., Bauer, P., Bechtold, P., Beljaars, a. C. M., van de Berg, L., Bidlot, J., Bormann, N., Delsol, C., Dragani, R., Fuentes, M., Geer, a. J., Haimberger, L., Healy, S. B., Hersbach, H., Hólm, E. V., Isaksen, L., Kållberg, P., Köhler, M., Matricardi, M., Mcnally, a. P., Monge-Sanz, B. M., Morcrette, J. J., Park, B. K., Peubey, C., de Rosnay, P., Tavolato, C., Thépaut, J. N. and Vitart, F.: The ERA-Interim reanalysis: Configuration and performance of the data assimilation system, Q. J. R. Meteorol. Soc., 137(April), 553–597, doi:10.1002/qj.828, 2011.

Degruyter, W. and Bonadonna, C.: Improving on mass flow rate estimates of volcanic eruptions, Geophys. Res. Lett., 39(May), 1–6, doi:10.1029/2012GL052566, 2012.

Dellino, P., Mele, D., Bonasia, R., Braia, G., La Volpe, L. and Sulpizio, R.: The analysis of the influence of pumice shape on its terminal velocity, Geophys. Res. Lett., 32(October), 1–4, doi:10.1029/2005GL023954, 2005.

Atmospheric
Chemistry
and Physics
Discussions

Open Access

1   Devenish, B. J., Francis, P. N., Johnson, B. T., Sparks, R. S. J. and Thomson, D. J.: Sensitivity analysis of
2   dispersion modeling of volcanic ash from Eyjafjallajökull in May 2010, J. Geophys. Res. Atmos., 117(D20),
3   n/a–n/a, doi:10.1029/2011JD016782, 2012.

4   Draxler, R. R. and Hess, G. D.: An Overview of the HYSPLIT_4 Modelling System for Trajectories, Dispersion,
5   and Deposition., Aust. Meteorol. Mag., 47(June 1997), 295–308, 1998.

6   Ferrier, B., Jin, Y., Lin, Y., Black, T., Rogers, E. and DiMego, G.: Implementation of a new frid-scale cloud and
7   precipitation shceme in the NCEP Eta Model, in Proc. 15th Conf. on Numerical Weather Prediction; San
8   Antonio; 12–16 August 2002; TX, pp. 280–283, American Meteorological Society., 2002.

9   Folch, A.: A review of tephra transport and dispersal models: Evolution, current status, and future perspectives,
10 J. Volcanol. Geotherm. Res., 235-236, 96–115, doi:10.1016/j.jvolgeores.2012.05.020, 2012.

11 Folch, A., Costa, A. and Macedonio, G.: FALL3D: A computational model for transport and deposition of
12 volcanic ash, Comput. Geosci., 35, 1334–1342, doi:10.1016/j.cageo.2008.08.008, 2009.

13 Folch, A., Costa, A. and Macedonio, G.: A model for wet aggregation of ash particles in volcanic plumes and
14 clouds: 1. Theoretical formulation, J. Geophys. Res. Solid Earth, 115, 1–16, doi:10.1029/2009JB007175, 2010.

15 Folch, A., Costa, A. and Macedonio, G.: FPLUME-1.0: An integrated volcanic plume model accounting for ash
16 aggregation, Geosci. Model Dev. Discuss., 8(9), 8009–8062, doi:10.5194/gmdd-8-8009-2015, 2015.

17 Gadd, A.: An economical explicit integration scheme. Tech. Note 44. UK Meteorological Office., 1974.

18 Ganser, G. H.: A rational approach to drag prediction of spherical and nonspherical particles, Powder Technol.,
19 77(2), 143–152, doi:http://dx.doi.org/10.1016/0032-5910(93)80051-B, 1993.

20 Girault, F., Carazzo, G., Tait, S., Ferrucci, F. and Kaminski, É.: The effect of total grain-size distribution on the
21 dynamics of turbulent volcanic plumes, Earth Planet. Sci. Lett., 394, 124–134, doi:10.1016/j.epsl.2014.03.021,
22 2014.

23 Grell, G. and Baklanov, A.: Integrated modeling for forecasting weather and air quality: A call for fully coupled
24 approaches, Atmos. Environ., 45(38), 6845–6851, doi:10.1016/j.atmosenv.2011.01.017, 2011.

25 Grell, G. a., Knoche, R., Peckham, S. E. and McKeen, S. a.: Online versus offline air quality modeling on cloud-
26 resolving scales, Geophys. Res. Lett., 31(April), 6–9, doi:10.1029/2004GL020175, 2004.

27 Grell, G. a., Peckham, S. E., Schmitz, R., McKeen, S. a., Frost, G., Skamarock, W. and Eder, B.: Fully coupled
28 "online" chemistry within the WRF model, Atmos. Environ., 39, 6957–6975,
29 doi:10.1016/j.atmosenv.2005.04.027, 2005.

30 Guffanti, M., Mayberry, G. C., Casadevall, T. and Wunderman, R.: Volcanic hazards to airports, Nat. Hazards,
31 51(2), 287–302, doi:10.1007/s11069-008-9254-2, 2009.

32 Janjic, Z.: Pressure gradient force and advection scheme used for forecasting with steep and small scale
33 topography, Beiträge zur Phys. der Atmosphäre, 50(1), 186–199, 1977.

34 Janjic, Z.: Forward-backward scheme modified to prevent two-grid-interval noise and its application in sigma

1   coordinate models, Contrib. Atmos. Phys, 52, 69–84, 1979.

2   Janjic, Z.: Nonlinear Advection Schemes and Energy Cascade on Semi-Staggered Grids, Mon. Weather Rev.,
3   112, 1234–1245, doi:10.1175/1520-0493(1984)112<1234:NASAEC>2.0.CO;2, 1984.

4   Janjic, Z.: The Step-Mountain Coordinate: Physical Package, Mon. Weather Rev., 118(7), 1429–1443,
5   doi:10.1175/1520-0493(1990)118<1429:TSMCPP>2.0.CO;2, 1990.

6   Janjic, Z.: The Step-Mountain Eta Coordinate Model: Further Developments of the Convection, Viscous
7   Sublayer, and Turbulence Closure Schemes, Mon. Weather Rev., 122(5), 927–945, doi:10.1175/1520-
8   0493(1994)122<0927:TSMECM>2.0.CO;2, 1994.

9   Janjic, Z.: The Mellor-Yamada level 2.5 turbulence closure scheme in the NCEP Eta Model, WORLD Meteorol.
10   Organ. TD, 4–14, 1996.

11   Janjic, Z.: Nonsingular Implementation of the Mellor-Yamada Level 2.5 Scheme in the NCEP Meso model,
12   Natl.   Centers   Environ.   Predict.,   61   [online]   Available   from:
13   http://www.emc.ncep.noaa.gov/officenotes/newernotes/on437.pdf, 2001.

14   Janjic, Z.: A nonhydrostatic model based on a new approach, Meteorol. Atmos. Phys., 82, 271–285,
15   doi:10.1007/s00703-001-0587-6, 2003.

16   Janjic, Z.: A unified model approach from meso to global scales, in EGU General Assembly Conference
17   Abstracts, vol. 7, European Geosciences Union 2005., 2005.

18   Janjic, Z. and Black, T.: An ESMF unified model for a broad range of spatial and temporal scales, in EGU
19   General Assembly Conference Abstracts, vol. 9, European Geosciences Union 2007., 2007.

20   Janjic, Z. and Gall, R.: Scientific documentation of the NCEP nonhydrostatic multiscale model on the B grid
21   (NMMB). Part 1 Dynamics, , (April), 72, doi:10.5065/D6WH2MZX, 2012.

22   Janjic, Z., Gerrity, J. and Nickovic, S.: An Alternative Approach to Nonhydrostatic Modeling, Part III: Nonlinear
23   Mountain Wave Test, World Meteorol. Organ. TD, 5–15, 2000.

24   Janjic, Z., Huang, H. and Lu, S.: A unified atmospheric model suitable for studying transport of mineral aerosols
25   from meso to global scales, IOP Conf. Ser. Earth Environ. Sci., 7, 012011, doi:10.1088/1755-1307/7/1/012011,
26   2009.

27   Janjic, Z., Janjic, T. and Vasic, R.: A Class of Conservative Fourth-Order Advection Schemes and Impact of
28   Enhanced Formal Accuracy on Extended-Range Forecasts, Mon. Weather Rev., 139(1973), 1556–1568,
29   doi:10.1175/2010MWR3448.1, 2011.

30   Jay, J., Costa, F., Pritchard, M., Lara, L., Singer, B. and Herrin, J.: Erratum to "Locating magma reservoirs using
31   InSAR and petrology before and during the 2011-2012 Cordón Caulle silicic eruption," Earth Planet. Sci. Lett.,
32   395, 254–266, doi:10.1016/j.epsl.2014.07.021, 2014.

33   Jöckel, P., von Kuhlmann, R., Lawrence, M. G., Steil, B., Brenninkmeijer, C. M., Crutzen, P. J., Rasch, P. J. and
34   Eaton, B.: On a fundamental problem in implementing flux-form advection schemes for tracer transport in 3-
35   dimensional general circulation and chemistry transport models, Q. J. R. Meteorol. Soc., 127(September 2015),

Atmospheric
Chemistry
and Physics
Discussions

1   1035–1052, doi:10.1002/qj.49712757318, 2001.

2   Jorba, O., Dabdub, D., Blaszczak-Boxe, C., Pérez, C., Janjic, Z., Baldasano, J. M., Spada, M., Badia, A. and

3   Gonçalves, M.: on global air quality with the NMMB/BSC chemical transport model, J. Geophys. Res.,

4   117(August), doi:10.1029/2012JD017730, 2012.

5   Lin, J. C.: Lagrangian Modeling of the Atmosphre: An Introduction, in Lagrangian Modeling of the Atmosphere,

6   pp. 1–11, American Geophysical Union., 2012.

7   Lorenz, E. N.: Energy and numerical weather prediction, Tellus, 12, 364–373, 1960.

8   Mastin, L. G., Guffanti, M., Servranckx, R., Webley, P., Barsotti, S., Dean, K., Durant, A., Ewert, J. W., Neri,

9   A., Rose, W., Schneider, D., Siebert, L., Stunder, B., Swanson, G., Tupper, A., Volentik, A. and Waythomas, C.

10   F.: A multidisciplinary effort to assign realistic source parameters to models of volcanic ash-cloud transport and

11   dispersion during eruptions, J. Volcanol. Geotherm. Res., 186(1-2), 10–21,

12   doi:10.1016/j.jvolgeores.2009.01.008, 2009.

13   Mastin, L. G., Van Eaton, A. and Lowenstern, J.: Modeling ash fall distribution from a Yellowstone

14   supereruption, Geochemistry, Geophys. Geosystems, 15(8), 3459–3475, doi:10.1002/2014GC005469, 2014.

15   Mellor, G. L. and Yamada, T.: Development of a turbulence closure model for geophysical fluid problems, Rev.

16   Geophys., 20(4), 851–875, doi:10.1029/RG020i004p00851, 1982.

17   Mesinger, F.: Forward-backward scheme, and its use in a limited area model., Beitr. Phys. Atmos., 50, 200–210,

18   1977.

19   Mlawer, E., Taubman, S., Brown, P., Iacono, M. and Clough, S.: Radiative transfer for inhomogeneous

20   atmospheres: RRTM, a validated correlated-k model for the longwave, J. Geophys. Res. Atmos., 102(D14),

21   16663–16682, doi:10.1029/97JD00237, 1997.

22   Monin, A. S. and Obukhov, A. M.: Basic laws of turbulent mixing in the surface layer of the atmosphere,

23   Contrib. Geophys. Inst. Acad. Sci. USSR, 24(151), 163–187, 1954.

24   Myhre, G., Shindell, D., Bréon, F. M., Collins, W., Fuglestvedt, J., Huang, J., Koch, D., Lamarque, J.-F., Lee,

25   D., Mendoza, B., Nakajima, T., Robock, A., Stephens, G., Takemura, T. and Zhan, H.: 2013: Anthropogenic and

26   Natural Radiative Forcing, Clim. Chang. 2013 Phys. Sci. Basis. Contrib. Work. Gr. I to Fifth Assess. Rep.

27   Intergov. Panel Clim. Chang., 659–740, doi:10.1017/ CBO9781107415324.018, 2013.

28   Osores, M. S., Folch, A., Ruiz, J. and Collini, E.: Estimación de alturas de columna eruptiva a partir de imáges

29   captadas por el sensor IMAGER del GOES-13, y su empleo para el pronóstico de dispersión y depóstio de

30   cenizas volcánicas sonre Argentina, in XIX Congreso Geologico Argentino., 2014.

31   Osores, M. S., Collini, E., Mingari, L., Folch, A., Ruiz, L., Toyos, G., Pujol, G., Farias, C., Alexander, P., Suaya,

32   M., Schonholz, T., Viramonte, J. G. and Villarosa, G.: Volcanic Ash Dispersion Modeling, Forecasting and

33   Remote Sensing in Argentina. Recent and future developments, in IUGG - VW04 Remote Sensing and

34   Modelling of Volcanic Ash in Latin America, International Union of Geodesy and Geophysics (IUGG), Czech

35   Republic., 2015.

Atmospheric
Chemistry
and Physics
Discussions

Pérez, C., Haustein, K., Janjic, Z., Jorba, O., Huneeus, N., Baldasano, J. M., Black, T., Basart, S., Nickovic, S., Miller, R. L., Perlwitz, J. P., Schulz, M. and Thomson, M. J.: Atmospheric dust modeling from meso to global scales with the online NMMB/BSC-Dust model; Part 1: Model description, annual simulations and evaluation, Atmos. Chem. Phys., 11, 13001–13027, doi:10.5194/acp-11-13001-2011, 2011.

Pfeiffer, T., Costa, A. and Macedonio, G.: A model for the numerical simulation of tephra fall deposits, J. Volcanol. Geotherm. Res., 140, 273–294, doi:10.1016/j.jvolgeores.2004.09.001, 2005.

Pistolesi, M., Cioni, R., Bonadonna, C., Elissondo, M., Baumann, V., Bertagnini, A., Chiari, L. and Gonzales, R.: Complex dynamics of small-moderate volcanic events : the example of the 2011 rhyolitic Cordón Caulle eruption , Chile, Bull. Volcanol., 77(3), doi:10.1007/s00445-014-0898-3, 2015.

Prata, A. J.: Infrared radiative transfer calculations for volcanic ash clouds, Geophys. Res. Lett., 16(11), 1293–1296, doi:10.1029/GL016i011p01293, 1989a.

Prata, A. J.: Observations of volcanic ash clouds in the 10-12 μm window using AVHRR/2 data, Int. J. Remote Sens., 10(4-5), 751–761, doi:10.1080/01431168908903916, 1989b.

Prata, A. J.: Volcanic Information Derived from Satellite Data., 2011.

Pyle, D.: The thickness, volume and grainsize of tephra fall deposits, Bull. Volcanol., 51(1), 1–15, doi:10.1007/BF01086757, 1989.

Raga, G. B., Baumgardner, D., Ulke, a. G., Torres Brizuela, M. and Kucienska, B.: The environmental impact of the Puyehue-Cordon Caulle 2011 volcanic eruption on Buenos Aires, Nat. Hazards Earth Syst. Sci., 13, 2319–2330, doi:10.5194/nhess-13-2319-2013, 2013.

Rood, R. B.: Numerical advection algorithms and their role in atmospheric transport and chemistry models, Rev. Geophys., 25(1), 71–100, doi:10.1029/RG025i001p00071, 1987.

Rose, W. and Durant, A.: Fine ash content of explosive eruptions, J. Volcanol. Geotherm. Res., 186(1-2), 32–39, doi:10.1016/j.jvolgeores.2009.01.010, 2009.

Schmid, R.: Descriptive nomenclature and classification of pyroclastic deposits and fragments, Geol. Rundschau, 70(2), 794–799, doi:10.1007/BF01822152, 1981.

Scollo, S., Del Carlo, P. and Coltelli, M.: Tephra fallout of 2001 Etna flank eruption: Analysis of the deposit and plume dispersion, J. Volcanol. Geotherm. Res., 160(1-2), 147–164, doi:10.1016/j.jvolgeores.2006.09.007, 2007.

Scollo, S., Kahn, R. A., Nelson, D. L., Coltelli, M., Diner, D. J., Garay, M. J. and Realmuto, V. J.: MISR observations of Etna volcanic plumes, J. Geophys. Res. Atmos., 117(6), 1–13, doi:10.1029/2011JD016625, 2012.

Self, S.: The effects and consequences of very large explosive volcanic eruptions., Philos. Trans. A. Math. Phys. Eng. Sci., 364(June), 2073–2097, doi:10.1098/rsta.2006.1814, 2006.

Simmons, a. J. and Burridge, D. M.: An Energy and Angular-Momentum Conserving Vertical Finite-Difference Scheme and Hybrid Vertical Coordinates, Mon. Weather Rev., 109, 758–766, doi:10.1175/1520-0493, 1981.

Atmospheric
Chemistry
and Physics
Discussions

1   Sommer, B.: Ash Cloud from Chilean volcano entering New Zealand Airspace, Civ. Aviat. Auth. New Zeal.

2   [online] Available from: https://www.caa.govt.nz/publicinfo/med_rel_Ash_Cloud.htm, 2011.

3   Spada, M., Jorba, O., Pérez, C., Janjic, Z. and Baldasano, J. M.: Modeling and evaluation of the global sea-salt

4   aerosol distribution: Sensitivity to emission schemes and resolution effects at coastal/orographic sites, Atmos.

5   Chem. Phys., 13, 11735–11755, doi:10.5194/acp-13-11735-2013, 2013.

6   Sparks, R. S. J., Bursik, M., Carey, S., Gilbert, J., Glaze, L., Sigurdsson, H. and Woods, A.: Volcanic Plumes, 1

7   edition., John Wiley, Chichester, U.K., 1997.

8   Stuefer, M., Freitas, S. R., Grell, G., Webley, P., Peckham, S. and McKeen, S. a.: Inclusion of Ash and SO_2

9   emissions from volcanic eruptions in WRF-CHEM: development and some applications, Geosci. Model Dev.

10   Discuss., 5, 2571–2597, doi:10.5194/gmdd-5-2571-2012, 2012.

11   Sulpizio, R., Folch, A., Costa, A., Scaini, C. and Dellino, P.: Hazard assessment of far-range volcanic ash

12   dispersal from a violent Strombolian eruption at Somma-Vesuvius volcano, Naples, Italy: Implications on civil

13   aviation, Bull. Volcanol., 74(9), 2205–2218, doi:10.1007/s00445-012-0656-3, 2012.

14   Suzuki, T.: A theoretical model for dispersion of tephra, Arc Volcanism Phys. Tectonics, 93–113, 1983.

15   Suzuki, Y. and Koyaguchi, T.: A three-dimensional numerical simulation of spreading umbrella clouds, J.

16   Geophys. Res., 114, 1–18, doi:10.1029/2007JB005369, 2009.

17   Vukovic, A., Rajkovic, B. and Janjic, Z.: Land Ice Sea Surface Model: Short Description and Verification, in

18   2010 International Congress on Environmental Modelling and Software Modelling for Environment's Sake,

19   Fifth Biennial Meeting, Ottawa, Canada, 5–8 July 2010., 2010.

20   Wessel, P. and Smith, W. H. F.: Free software helps map and display data, Eos, Trans. Am. Geophys. Union,

21   72(41), 441–441, doi:10.1029/90EO00319, 1991.

22   Wilson, L. and Huang, T. C.: The influence of shape on the atmospheric settling velocity of volcanic ash

23   particles, Earth Planet. Sci. Lett., 44(2), 311–324, doi:10.1016/0012-821X(79)90179-1, 1979.

24   Wilson, T., Stewart, C., Bickerton, H., Baxter, P., Outes, V., Villarosa, G. and Rovere, E.: Impacts of the June

25   2011 Puyehue-Cordón Caulle volcanic complex eruption on urban infrastructure, agriculture and public health.

26   GNS Science Report., 2013.

27   Woodhouse, M., Hogg, a. J., Phillips, J. C. and Sparks, R. S. J.: Interaction between volcanic plumes and wind

28   during the 2010 Eyjafjallajökull eruption, Iceland, J. Geophys. Res. Solid Earth, 118, 92–109,

29   doi:10.1029/2012JB009592, 2013.

30   Zhang, L., Gong, S., Padro, J. and Barrie, L.: A size-segregated particle dry deposition scheme for an

31   atmospheric aerosol module, Atmos. Environ., 35, 549–560, doi:10.1016/S1352-2310(00)00326-5, 2001.

32   Zilitinkevich, S.: Bulk characteristics of turbulence in the atmospheric planetary boundary layer, Tr. GGO, 167,

33   49–52, 1965.

34

Atmospheric
Chemistry
and Physics
Discussions

1

2   **Table 1. Main characteristics of the NMMB/BSC-ASH meteorological solver.**

Meteorological Solver	*Scheme*	*Reference*
Spatial discretization		
Multi-scale domain ranging from large eddy simulations (LES) to global simulations		Janjic (2005)
Conservativeness		
Conservation of mass, momentum, energy, enstrophy and a number of other first order and quadratic quantities. Positive definiteness and monotonicity are preserved by tracer advection		Janjic (1984)
Coordinates /Grid		
Horizontal coordinate	Rotated latitude-longitude for regional domains, and latitude-longitude coordinate with polar filter for global domains	Janjic et al. (2009); Janjic and Gall, (2012)
Vertical coordinate	Terrain following hybrid sigma-pressure	Simmons and Burridge, (1981)
Horizontal grid	Arakawa B-grid staggering	Janjic, 2005; Janjic and Black, 2007)
Vertical grid	Lorenz staggering	Lorenz, (1960)
Time integration schemes		
Horizontally propagating fast-waves	Forward-backward scheme	Ames, (1969); Gadd, (1974); Mesinger, (1977); Janjic, 1979)
Vertically propagating sound waves	Implicit scheme	Janjic and Gall, (2012)
Horizontal advection & Coriolis terms	Modified (Stable) Adams-Bashforth scheme	
Vertical advection	Crank-Nicholson scheme	Janjic, (1977,1984)
TKE generation and dissipation	Iterative	
Advection terms		
Horizontal	Energy and enstrophy conserving, quadratic conservative, second order	Janjic and Gall, (2012)
Vertical	Quadratic conservative, second order	Janjic and Gall, (2012)
Diffusion terms		
Vertical	Surface layer scheme	Janjic (1994, 1996)
Lateral	Smagorinsky non-linear approach	Janjic (1990)
Physics Options		
Microphysics/Clouds	Ferrier (Eta)	Ferrier et al. (2002)
Short and Longwave Radiation	Rapid Radiative Transfer Model (RRTM)	Mlawer et al. (1997); Pérez et al. (2011)
Surface Layer	NMMB similarity theory scheme: Based on Monin-Obukhov similarity theory with Zilitinkevich thermal roughness length	Monin and Obukhov (1954); (Zilitinkevich, 1965); Janjic (1994, 1996)
Land Surface, Heat & moisture surface flux	LISS model	Vukovic et al. (2010)
Planetary Boundary layer / free atmosphere	Mellor-Yamada-Janjic scheme	Mellor and Yamada, (1982); Janjic (1996, 2001)
Convective adjustments	Betts-Miller-Janjic scheme	Betts and Miller, (1986); Janjic (1994, 2000).

3

4

Atmospheric
Chemistry
and Physics
Discussions

1 **Table 2. Options implemented in NMMB/BSC-ASH to estimate the mass eruption rate from column height. Unless**
2 **otherwise noted, the units for all parameters are in SI.**

Reference	MER schemes	Eq.	Parameters
Mastin et al., (2009)	$MER = \bar{\rho}\left[\dfrac{0.5 H_{plume}}{10^3}\right]^{\frac{1}{0.241}}$	(1)	$\bar{\rho}$ = magma density (2500 kg m^{-3}) H_{plume} = column height
Degruyter and Bonadonna (2012)	$MER = \pi\dfrac{\rho_{a0}}{g'}\left(\dfrac{\alpha^2\bar{N}^3}{z_1^4 n}H_{plume}^4 + \dfrac{\beta^2\bar{N}^2\bar{v}}{6}H_{plume}^3\right)$ $g' = g\left(\dfrac{c_0\theta_0 - c_{a0}\theta_{a0}}{c_{a0}\theta_{a0}}\right)$ ρ_{a0} =1.105, α =0.1, β =0.5, z_1 =2.8; θ_0 =1200, θ_{a0} =268.7, $c0$ =1250, $ca0$ =998	(2)	ρ_{a0} = atmospheric density at the vent (kg m^{-3}) g' = reduced gravity $\bar{N}$ = average buoyancy frequency (s^{-1}) $\bar{v}$ = average wind velocity across column height (m s^{-1}) z_1 = Max. non-dimensional height α, β = radial and crossflow entrainment coefficients g = gravitational constant (9.81 m s^{-2}) c_0 = source specific heat (J kg^{-1} K^{-1}) c_{a0} = specific heat of the atmosphere (J kg^{-1} K^{-1}) θ_0 = source temperature (K) θ_{a0} = atmospheric temperature (K)
Woodhouse et al. (2013)	$MER = 0.35\alpha^2 f(W_s)^4\dfrac{\rho_{a0}}{g'}N^3 H_{plume}^4$ $f(W_s) = 1.44\dot{\gamma}/\bar{N}$ $g' = g\left(\dfrac{c_v n_0 + c_s(1-n_0)\theta_0 - c_a\theta_{a0}}{c_a\theta_{a0}}\right)$	(3)	Q = mass flux (kg s^{-1}) W_s = dimensionless wind strength $\bar{N}$ = average buoyancy frequency (s^{-1}) $\dot{\gamma}$ = shear rate of atmospheric wind (s^{-1}) c_s = specific heat of solids (J kg^{-1} K^{-1}) c_a c_s = specific heat of dry air (J kg^{-1} K^{-1}) = specific heat of water vapor (J kg^{-1} K^{-1})

3

4 **Table 3. Ash aggregation options in NMMB/BSC-ASH from analytical solutions based from field observations.**
5 **Default aggregate properties can be modified by the user.**

Name	New aggregate class	Default properties	Reference
NONE	No aggregation processes	n/a	n/a
CORNELL	50% of the 63–44 μm class aggregate 75% of the 44–31 μm class aggregate 100% of the < 31 μm class aggregate	Diameter = 250 μm Density = 350 kg m^{-3} Sphericity = 0.9	Based on Cornell et al. (1983) Campanian Ignimbrite's deposit (Y5 ash layer)
PERCENTAGE	Takes a user-defined fixed percentage from each particle class	Diameter = 250 μm Density = 350 kg m^{-3}	Based on Sulpizio et al. (2012)

6

7 **Table 4. Governing equations for NMMB/BSC-ASH wet aggregation model.**

	Wet aggregation scheme	Eq.	Parameters
Number of particles of a class aggregated	$\Delta n_f \approx \dfrac{\Delta n_{tot} N_j}{\sum_k N_k}$ $(k = k_{min}, \ldots, k_{max})$	(5)	Δn_{tot} = number of particles that aggregate per time interval N_j = number of particles of diameter j in an aggregate N_k = number of particles in an aggregate

Atmospheric
Chemistry
and Physics
Discussions

Open Access

	Number of particles aggregated during Δt	$N_j = k_f \left(\dfrac{d_A}{d_j}\right)^{D_f}$	(6)	k_f = fractal prefactor ≈ 1 D_f = fractal exponent ≤ 3 d_A = aggregate diameter d_j = primary particle diameter
	Total particle decay per unit volume during Δt	$\Delta n_{tot} = \alpha_m \left((A_B n_{tot}^2 + A_S \emptyset^{3/D_f} n_{tot}^{2-3/D_f} + A_{DS} \emptyset^{4/D_f} n_{tot}^{2-4/D_f}) \Delta t \right.$	(7)	α_m = mean sticky efficiency $\emptyset$ = solid volume fraction
	Number of particles available to aggregate	$n_{tot} = \sum_j \dfrac{6 C_j}{\pi \rho_j d_j^3}$	(8)	n_{tot} = number of particles available to aggregate k_b = is the Boltzmann constant 1.38×10^{-23} m^2 kg s^{-2} K T = absolute temperature μ_o = dynamic viscosity of air
	Kernels	For Brownian motion: $A_B = -\dfrac{4 k_b T}{3 \mu_o}$ Ambient fluid shear: $A_S = \dfrac{2 \Gamma_S \varepsilon^4}{3}$ Differential sedimentation: $A_{DS} = -\dfrac{\pi (\rho_m - \rho_a) g \varepsilon^4}{48 \mu_o}$		Γ_S = fluid shear ε = particle diameter to volume fractal relationship ρ_m = mean particle density ρ_a = air density

1

2 **Table 5. Governing equations for NMMB/BSC-ASH gravity current model .**

	Gravity current scheme	*Eq.*	*Parameters*
Effective radial velocity of the umbrella spreading	$u_b(t) = \dfrac{2}{3}\left(\dfrac{3\lambda N q}{2\pi}\right)^{1/3} t^{1/3}$ $u_b(R) = \left(\dfrac{2\lambda N q}{3\pi}\right)^{1/2} \dfrac{1}{\sqrt{R}}$	(9)	u_b = effective radial velocity as a function of time (t) or cloud radius (R) λ = empirical constant ($\lambda \approx 0.2$) (Suzuki and Koyaguchi, 2009) N = Brunt-Väisälä frequency (atm. ambient stratification) q = volumetric flow rate into the umbrella region

Volumetric flow rate into the umbrella region	$q = C\sqrt{k}\dfrac{M^{3/4}}{N^{5/8}}$
	
	 $C \begin{cases} 0.5 \times 10^4 \text{ m}^3 \text{ kg}^{-3/4} \text{ s}^{-7/8} \\ 1.0 \times 10^4 \text{ m}^3 \text{ kg}^{-3/4} \text{ s}^{-7/8} \end{cases}$
		(10)	M = efficiency of air entrainment
			 k = mass eruption rate
			 C = location base constant
			    C_A : for tropical eruptions
			    C_B : for midlatitude and polar eruptions

Contribution of the gravitational spreading	$ct = \left(\dfrac{u_b}{u_b + u_w}\right) \times 100$	(11)	u_w = wind field velocity

Radial distance (gravity vs. passive transport)	$Ri = \dfrac{u_b^2}{u_w^2} = \dfrac{4}{9 u_w^2}\left(\dfrac{3\lambda N q}{2\pi}\right)^{2/3} t^{-2/3}$	(12)	Ri = Richardson number
			    $Ri > 1$: gravity-driven regime
			    $Ri < 0.25$: passive transport regime

3

4 **Table 6. Settling velocity models in NMMB/BSC-ASH.**

NAME/Reference	*Drag coefficient*	*Eq.*	*Description/ Parameters*
ARASTOOPOUR (Arastoopour et al., 1982)	$C_d = \begin{cases} \dfrac{24}{Re}\{1 + 0.15 Re^{0.687}\} & Re \leq 988.947 \\\\ 0.44 & Re > 988.947 \end{cases}$	(14)	For spherical particles only

GANSER (Ganser, 1993)	$C_d = \dfrac{24}{Re K_1}\{1 + 0.1118[Re(K_1 K_2)]^{0.6567}\} + \dfrac{0.4305 K_2}{1 + \dfrac{3305}{Re K_1 K_2}}$	(15)	For spherical and non-spherical particles
	$K_1 = \dfrac{3}{[(d_n/d)] + 2\psi^{-0.5}}$; $K_2 = 10^{1.8148(-Log\psi)^{0.5743}}$		K_1, K_2 = shape factors d_n = average between the min. and max. d axis ψ_{work} = sphere volume = particle sphericity (ψ= 1 for spheres)
	$\psi_{\text{work}} = 12.8 \dfrac{(P^2 Q)^{1/3}}{1 + P(1 + Q) + 6\sqrt{1 + P^2(1 + Q^2)}}$		
WILSON (Pfeiffer et al., 2005; Wilson and Huang, 1979)	$C_d = \begin{cases} \dfrac{24}{Re}\varphi^{-0.828} + 2\sqrt{1.07 - \varphi} & Re \le 10^2 \\ 1 - \dfrac{1 - C_d|_{Re=10^2}}{900}(10^3 - Re) & 10^2 \le Re \le 10^3 \\ 1 & Re \le 10^3 \end{cases}$	(16)	ψ = particle aspect ratio $\psi = (b + c)2a^{-1}$ a, b, c = particle semi-axes
DELLINO (Dellino et al., 2005)	$v_s = 1.2605 \dfrac{v_a}{d}(Ar\varepsilon^{1.6})^{0.5206}$ $Ar = gd^3(\rho_p - \rho_a)\rho_a/\mu_a^2$	(17)	For larger particles only Ar = Archimedes number g = gravity acceleration ε = particle shape factor μ_a = dynamic viscosity d = particle equivalent diameter, ρ_p = particle density ρ_a = air density

1

2 **Table 7. Model configuration for the 2011 Cordón Caulle regional and global runs. The regional run used a horizontal**
3 **resolution of 0.15º x 0.15º with a 30s dynamic time-step, while the global domain used a horizontal resolution of 1º x**
4 **0.75º with a 180s dynamic time-step.**

MODEL CONFIGURATION	
Dynamics	NMMB (30s/180s time-step)
Physics	Ferrier microphysics BMJ cumulus scheme MYJ PBL scheme LISS land surface model
Aerosols	11 ash bins (30s/180s time-step)
Source Term (emissions)	
Duration	20 days
Vertical distribution	Suzuki distribution
MER formulation	Mastin et al. (2009)
Aggregation model	Percentage
Sedimentation model	Ganser (1993)
Run Set-up	
Number of processors	512
Domain	Regional/Global
Horizontal resolution	0.15º x 0.15º / 1º x 0.75º
Vertical layers	60
Top of the atmosphere	21 hPa
Meteorology Boundary conditions (spatial resolutions)	ECMWF EraInterim Reanalysis (0.75º x 0.75º)

Atmospheric
Chemistry
and Physics
Discussions

1

2   **Table 8. Model configuration for the 2001 Mt. Etna regional simulations. Regional Run1 used a horizontal resolution**
3   **of 0.1° x 0.1° with a 30s dynamic time-step, while Run2 used a finer horizontal resolution of 0.05° x 0.05° with a 10s**
4   **dynamic time-step.**

Source Term (emissions)	
Duration	3 days
Vertical distribution	Suzuki distribution
MER formulation	Mastin
Column height	2570
Ash bins	8
Aggregation model	Cornell et al. (1983)
Sedimentation model	Ganser (1993)
Run Set-up	
Number of processors	256
Domain	Regional 1 / Regional 2
Horizontal resolution	0.1° x 0.1° / 0.05° x 0.05°
Vertical layers	60
Top of the atmosphere	21 hPa
Meteorology Boundary conditions (spatial resolutions)	ECMWF EraInterim Reanalysis (0.75° x 0.75°)

5
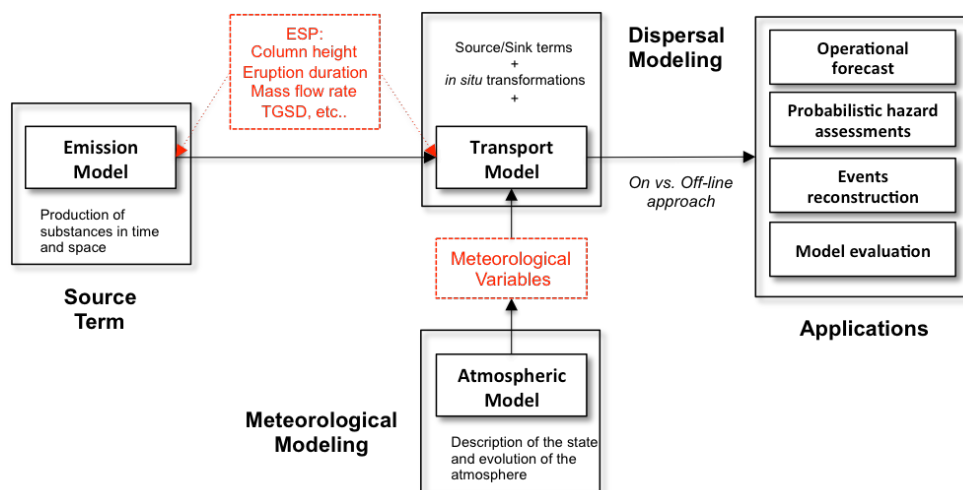
6

7   **Figure 1. Schematic representation of the main components of an Atmospheric Transport Model. Red text shows**
8   **model specifications for the transport of volcanic ash.**
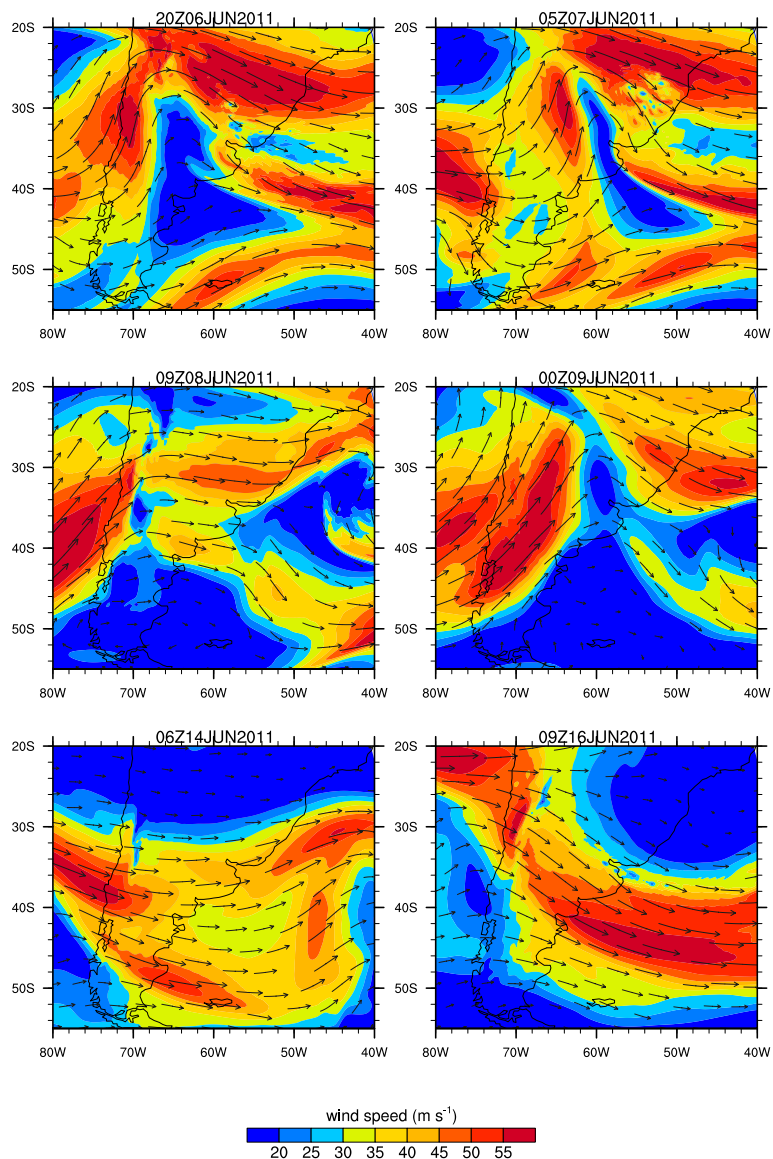
Figure 2. Meteorological synoptic situation over Europe during 6-16 June. Plots show the direction (vector) and velocity (contours m s⁻¹) of the wind at 9100 m above ground level (300 hPa circa). Meteorological data obtained from the NMMB meteorological forecast driven with ERA-Interim reanalysis at 0.75º horizontal resolution.

Atmospheric
Chemistry
and Physics
Discussions
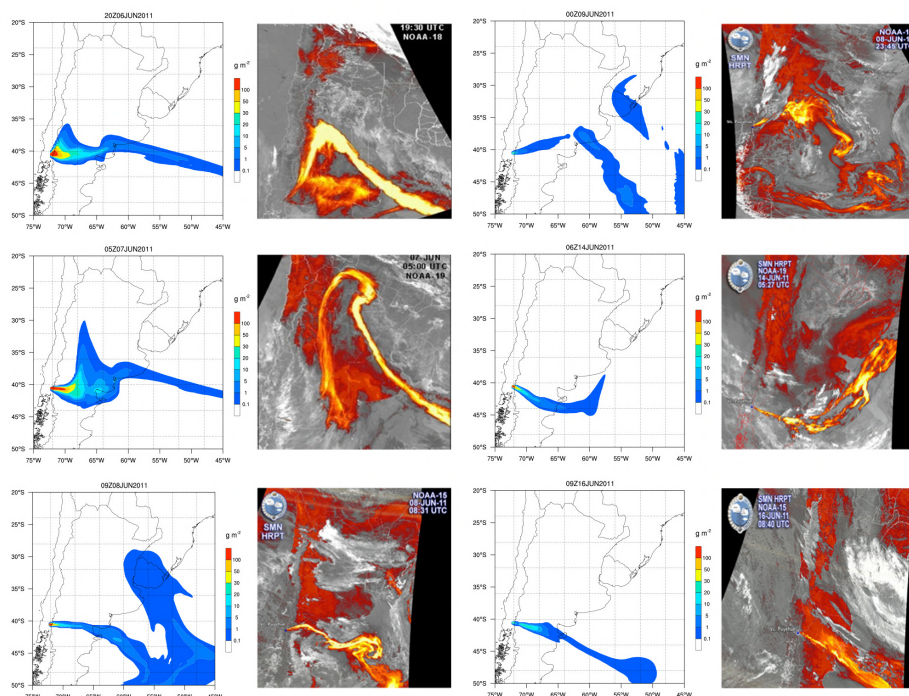
1

2 **Figure 3. Composite image of NMMB/BSC-ASH results for dispersion of ash for the 2011 Caulle eruption at different**
3 **time slices. Simulation results are compared against split windows algorithm NOAA-AVHRR satellite images.**
4 **Contours indicate ash column load (g m^{-2}) resulting from integrating the mass of the ash cloud along the atmospheric**
5 **vertical levels.**

6

Atmospheric
Chemistry
and Physics
Discussions

Open Access

EGU
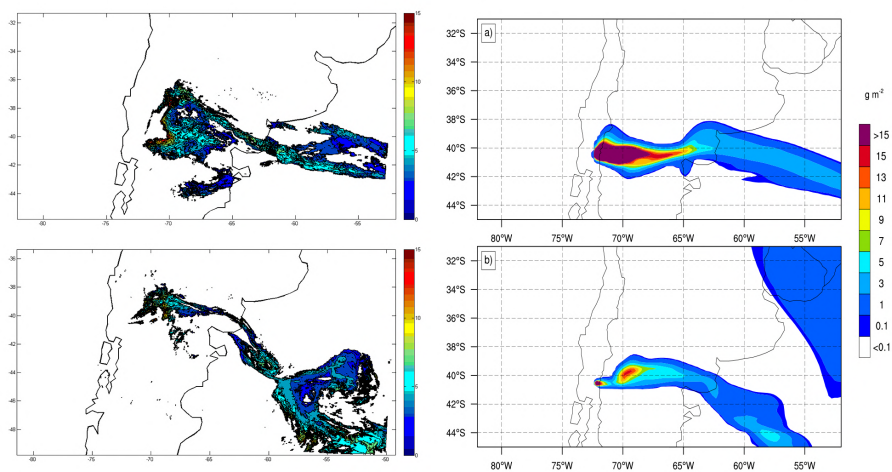
1

2   **Figure 4. Left: Mass loadings of the 2011 Caulle volcanic ash cloud from the MODIS-based retrievals (Osores et al.,**
3   **2015). Right: Predicted column mass (g m^{-2}) with NMMB/BSC-ASH for a) 6 June at 14:25 UTC and, b) 8 June at**
4   **14:15 UTC.**

5

1
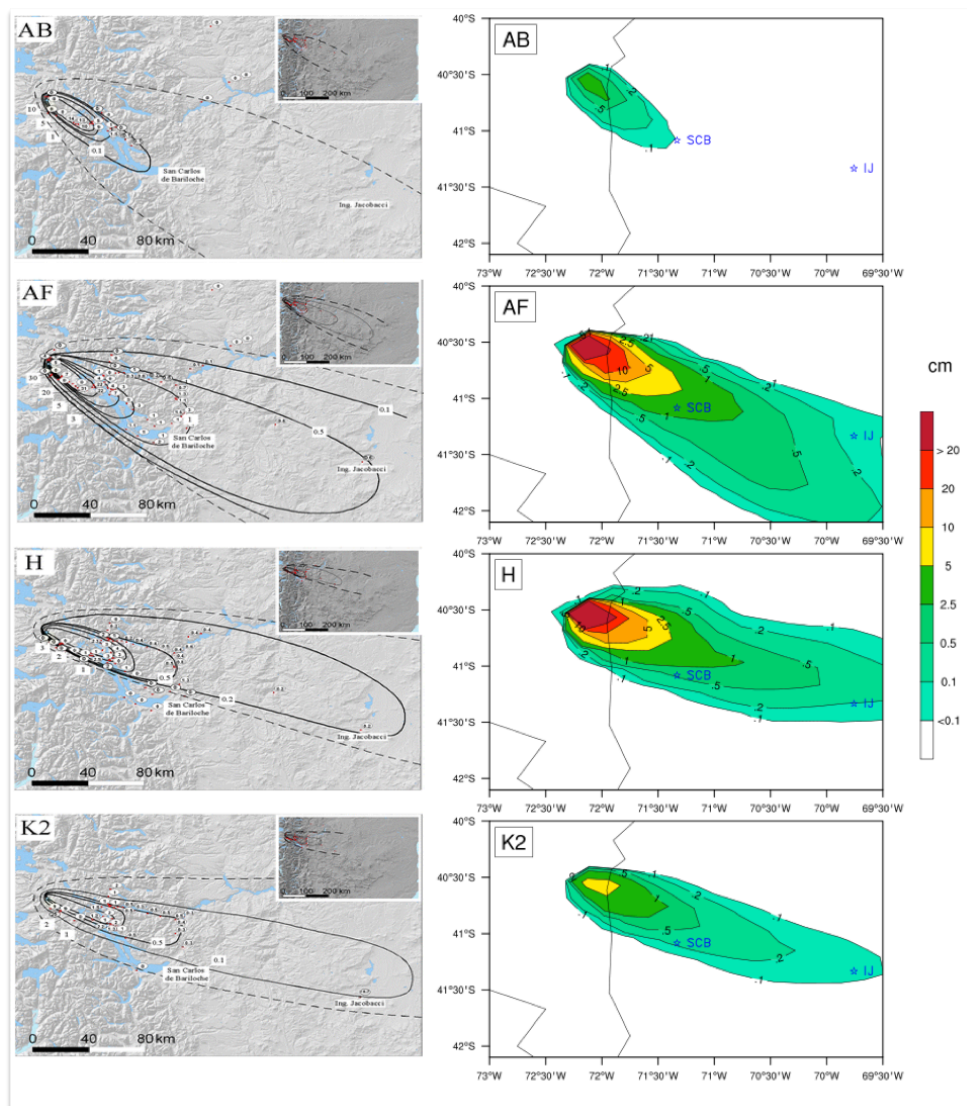
Figure 5. Left: Isopach maps in centimeter of layers A-B, A–F, H, and K2. Dashed lines infer the limit of the deposits presented in Pistolesi et al. (2015b). Right: Corresponding NMMB/BSC-ASH computed thicknesses (cm). Key locations in blue include San Carlos de Bariloche (SCB) and Ingeniero Jacobacci (IJ), 90 and 240 km east of the vent)

5

Atmospheric
Chemistry
and Physics
Discussions

Open Access

EGU
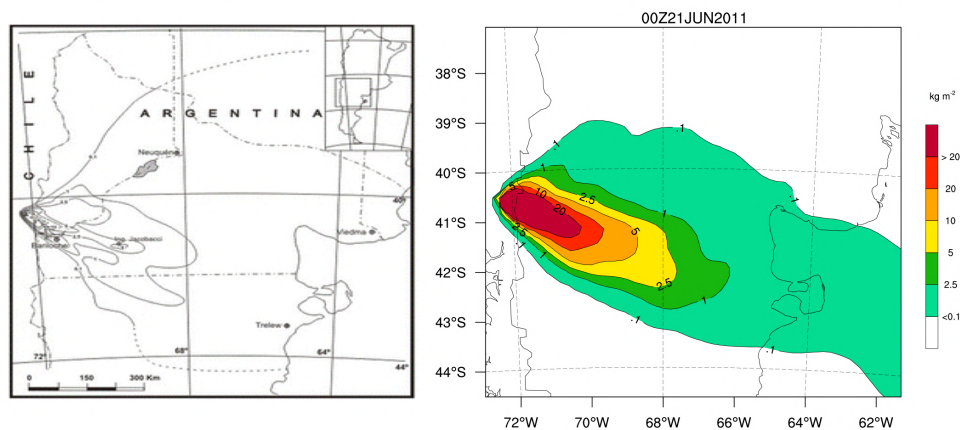
Figure 6. Left: measured ground deposit isopachs (kg m^{-2}) for the period beginning on 4 June until 30 June. Dashed lines infer the limit of the deposits (Collini et al., 2013). Right: Predicted deposit load (kg m^{-2}) with NMMB/BSC-ASH at the end of the simulation. Key locations in blue include San Carlos de Bariloche (SCB; 90 km from the vent), Ingeniero Jacobacci (IJ; 240 km east of the vent), and Trelew and Viedma (~ 600 km SE and NE of the vent, respectively).

1
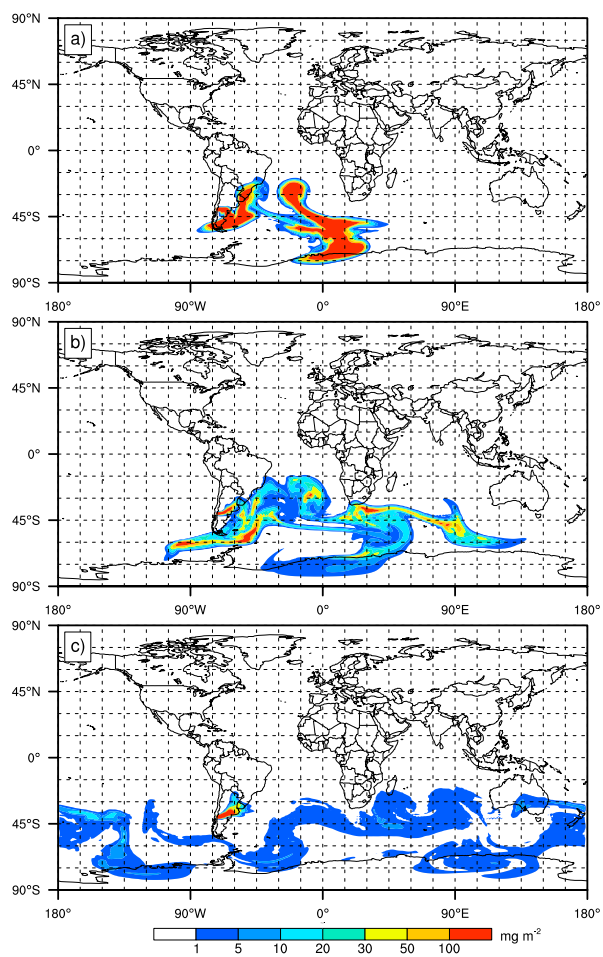
Figure 7. NMMB/BSC-ASH total column concentration (mass loading; mg m^{-2}) from our global simulation. Results
for a) 8 June at 09:00 UTC, b) 10 June at 04:00 UTC, and c) 14 June at 06:00 UTC.

Atmospheric
Chemistry
and Physics
Discussions

1
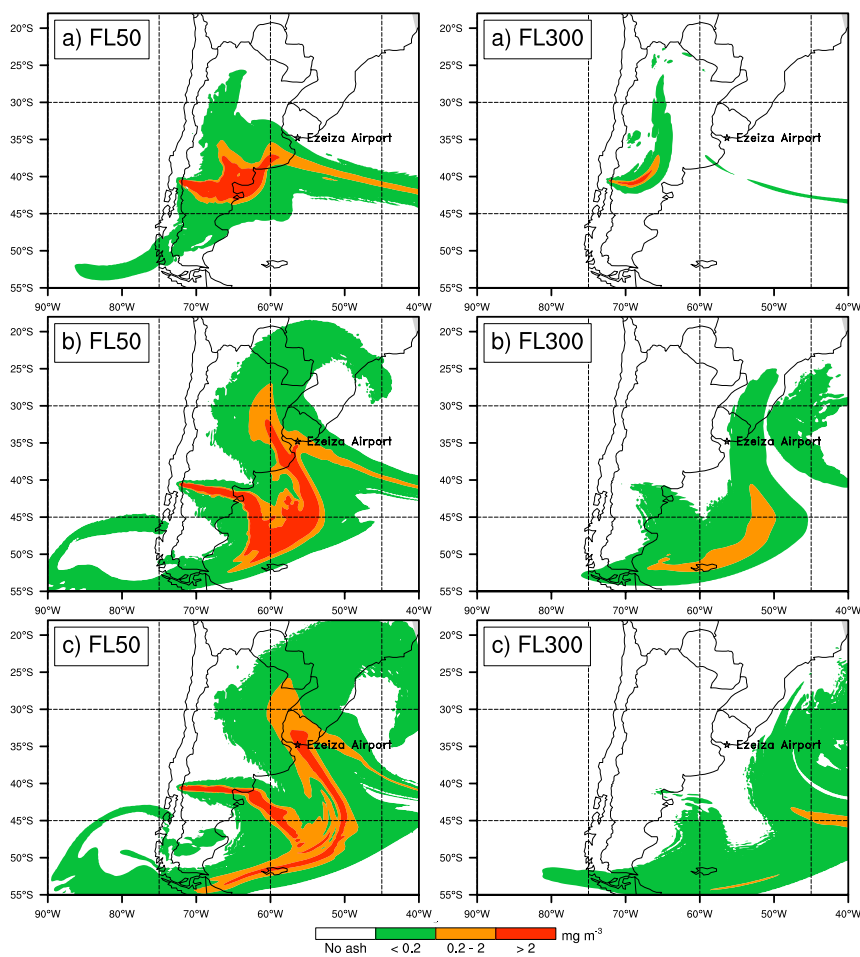
Figure 8. NMMB/BSC-ASH Flight level ash concentrations (mass loading; mg m^{-3}) before and after closure of the Buenos Aires (Ezeiza) airport and air space. Results for FL50 (left) and FL300 (right) for a) 6 June at 11:00 UTC, b) 7 June at 04:00 UTC, and c) 7 June at 12:00 UTC. Safe ash concentration thresholds are shown (red contours illustrate "No Flying" zones).

6

Atmospheric
Chemistry
and Physics
Discussions

1
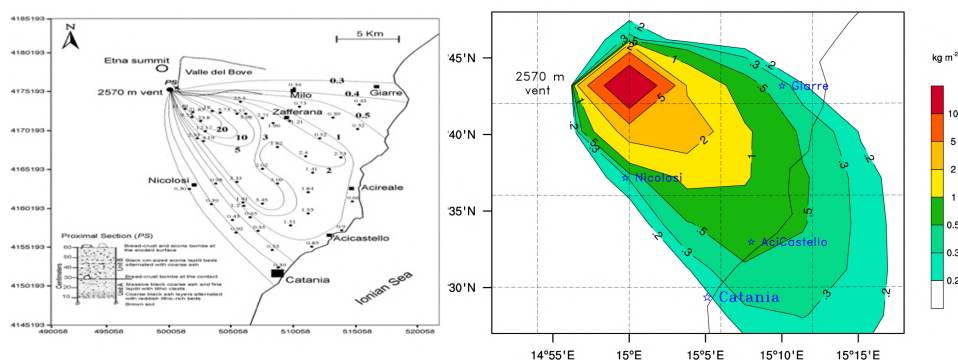
Figure 9. Left: Isomass map of the tephra deposit formed between 21 and 24 July 2001. Curves are given in kg m⁻². Coordinates are given in UTM-Datum ED50 (Scollo et al., 2007). Right: Predicted deposit load (kg m⁻²) with NMMB/BSC-ASH at the end of the event.

5

6
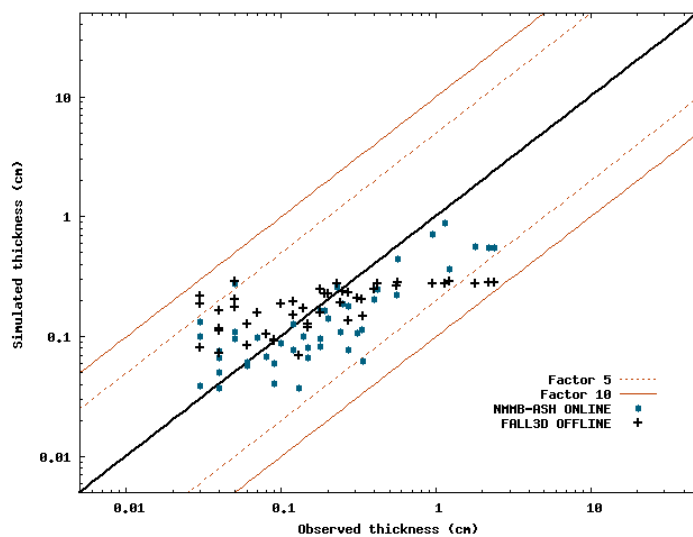
Figure 10. Simulated versus observed thicknesses for the reconstruction of the 2011 Etna eruption with NMMB-ASH (circles) and FALL3D (crosses). The solid bold line represents a perfect agreement, while the dashed and solid thin orange lines mark the region that is different from observed thicknesses by a factor 5 (1/5) and 10 (1/10), respectively

10   .

Atmospheric
Chemistry
and Physics
Discussions

Open Access
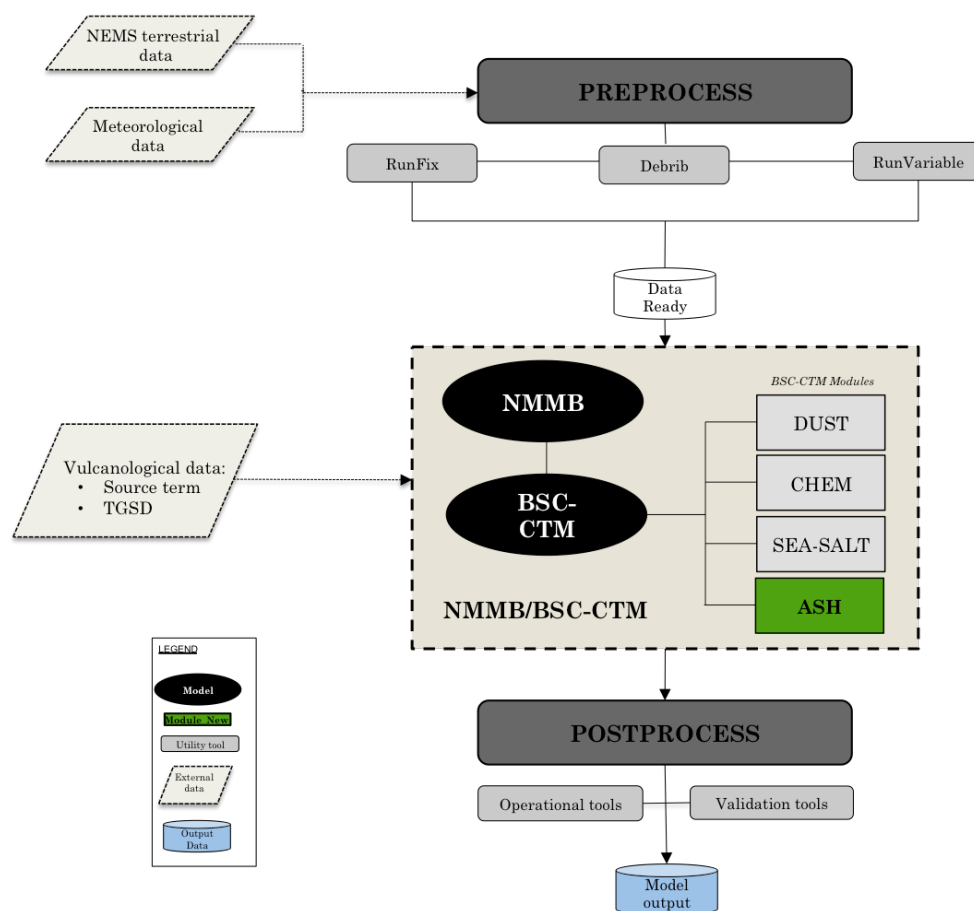
1
2   **Figure 11. Schematic representation of the operational implementation of NMMB/BSC-ASH.**

3

Atmospheric
Chemistry
and Physics
Discussions

1
2
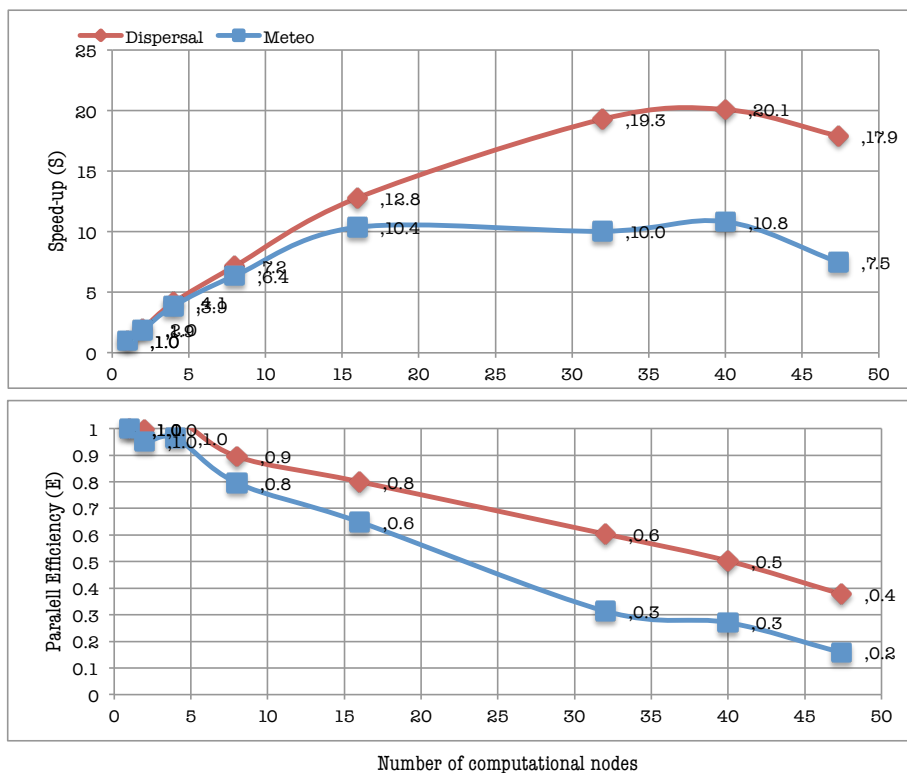
Figure 12. Figure NMMB/BSC-ASH scalability results. Top: parallel speed-up (S; computational speed) for meteorology only (blue) and for meteorology and dispersal combined (red). Bottom: parallel efficiency (E) versus number of computation nodes employed.

6

Atmospheric
Chemistry
and Physics
Discussions

Open Access

EGU

1
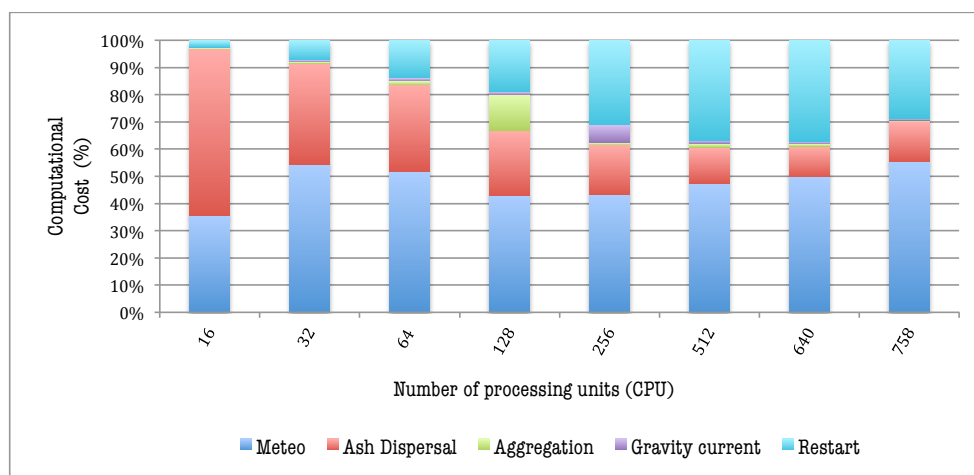
Figure 13. NMMB/BSC-ASH relative computational cost (%) with increasing CPUs. Represented processes include:
Meteorology (blue); Ash dispersal for 10 bins (red); Aggregation (green); Gravity current (purple) and; Restart (light
blue).